Simulation of Coupled Electrostatic Mechanical Behavior with the Finite Element Method

Lan Jin

Supervisors: Dr. P.D. Ledger and Dr. A.J. Gil

Project Dissertation submitted to the University of Wales Swansea in Partial Fulfilment for the Degree of Master of Science

Civil and Computational Engineering Center

Swansea University

June, 2010

Declarations and Statements

This work has not previously been accepted in substance for any degree and is not being concurrently submitted in candidature for any degree.

signed

Date

This dissertation is the result of my own independent work/investigation, except where otherwise stated. Other sources are acknowledged by footnotes giving explicit references. A bibliography is appended.

signed

Date

I hereby give consent for my dissertation, if relevant and accepted, to be available for photocopying and for inter-library loan, and for the title and summary to be made available to outside organizations.

signed

Date

Acknowledgments

First, I would like to express my deepest gratitude to my thesis supervisors, Dr. P.D. Ledger and Dr. A.J. Gil. I learnt a lot from them and I really enjoyed working with them. They spent a lot of time also on reading and improving my thesis. They have made me improved a lot. Secondly, I would like to thank my boyfriend, Xiong and my parents for their love, encouragement and continuous support. They helped me go through the tough time of thesis writing. Thirdly, I would like to thank all my teachers and schoolmates for their valuable insights they shared with me. Finally, I would like to give my gratitude to Erasmus Mundus European Commission for giving me this great opportunity to study computational mechanics, travel different countries, and meet people from different culture. It is really a good experience for me.

Contents

Summary

Coupling behavior exists in every industrial field. There are various kinds of coupling, wherein coupling between electrostatic and mechanical fields is one of the most common. Electrostriction, one example of coupled electromechanical behavior, is one of fundamental properties of insular materials. The principle of coupling mechanism is: An electric field causes a deformation of the material and this leads to strains which in turn change the material properties and the deformation. Some of these materials such as EAP(Electro Active Polymers) is used in developing robotic arms, and piezoelectric ceramics or composites has been applied in precision machine tools, aviation actuators, medical imaging systems and bionics aircrafts. In these applications, electrostriction plays an very important role. In reality, however, it is challenging to understand these coupling behaviors properly from the analytical point of view. Therefore, appropriate numerical methods should be employed to model the coupling behavior accurately.

This thesis aims to generate an effective, efficient and robust finite element approach for two dimensional coupled electrostatic mechanical problem, in particular, for electrostriction. The task involves electric field simulation, mechanical field simulation, and finally electrostriction coupling simulation. When Poisson's ratio close to 0.5, there is volumetric locking in mechanical field with displacement finite element formulation, which may result in an inaccurate solution. In order to overcome locking, hp finite element method is chosen in this thesis, whose advantage is obtaining accurate results with either exponential or algebraic convergence rate. Also mixed finite element method is developed to overcome locking. Thus, we can combine hp with displacement or mixed finite element method to achieve accurate results.

In each stage of simulation, the performance of developed hp finite element methods are tested in some benchmark problems.

In conclusion, the developed hp finite element methods can model electric field, mechanical field accurately with good convergency. For the electrostriction benchmark problem, because of the lack of analytical solution, convergence couldn't be tested. However, with one way coupling algorithm of electrostriction, the developed hp methods present exponential convergence rate with p refinement.

Chapter 1

Introduction

1.1 Background

Frequently two or more physical systems interact with each other, with the independent solution of any one system being impossible without simultaneous solution of the others. Such systems are known as coupled systems[1]. The common systems of multi-physics (or coupled-physics)include such as electric-mechanical, fluid-structure, and thermal-mechanical interactions. The applications for multi-physics systems cover every industry, including automotive, aerospace, electronics, semiconductor, telecommunications, pharmaceutical, and biomedical. Many such applications include sensors, transducers, and actuators, where one physical phenomenon is converted into another: electricity into motion, for example, or fluid pressure into electricity[2]. Coupled electrostatic mechanical system is one of the common systems of multi-physics and has wider applications. To illustrate this, some application areas are now considered.

The micro-electro-mechanical system(MEMS) industry has grown

incredibly fast over the past few years. MEMS devices have been widely used in various industries such as aerospace, automobile and biomedical industries. Multi-physics systems are often present in MEMS. The coupling between electrostatic and mechanical fields is one of the most common and fundamental phenomena in MEMS. There are many types of microsensors and microactuators distinguished by the coupling between electrostatic and mechanical fields. These MEMS sensors and actuators have various applications. Micropumps, for example are widely used in transport of small accurately measured liquid and gas in chemical and biomedical fields[3, 4]; Micromirros are used in display technology and optical switches[5]; Comb-drive actuators are used in microgrippers and force-balanced accelerometers[6]; Microswitches[7] are used in microwave. These are shown in figure(1.1).

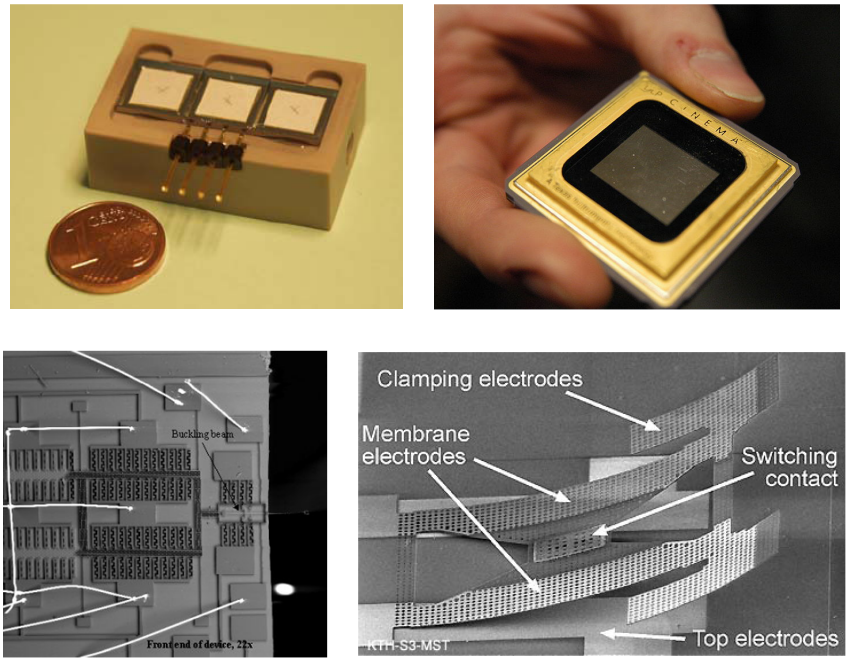

Figure 1.1: MEMS Engineering Applications, Micropumps, Micromirrors, Comb-drive actuaotrs, Microswitches

Moreover, the coupled electrostatic and mechanical behavior can be found in some kinds of material properties. Electrostriction,for example, is the fundamental mechanism of electromechanical coupling in all insulator materials[8]. An electric field applied to a dielectric produces a deformation which has been observed to be an even function of the intensity[9]. This is known as the electrostriction property of insulator materials. This property of materials can be applied in many industries. Smart materials like Electro Active Polymers (EAP)[10], exhibit large displacements, and change their mechanical behavior in response to the application of electric field. An important application of these smart materials can be found in developing robotic arms that are actuated by artificial muscles, where the smart materials are used as actuators. Piezoelectric ceramics or composites[11], because of its good dielectric and electrostriction properties, has been applied in precision machine tools, aviation actuators, medical imaging systems and bionics aircrafts.

Only a few applications for coupled electrostatic mechanical systems have been mentioned, but already it is possible to observe these applications are wide ranging and can be applied in various industries.

1.2 Numerical Methods

As discussed above, coupled electrostatic mechanical behavior can be found in the various industrial applications. Therefore, it is important to obtain an accurate prediction of the behavior of such coupling applications. However, modeling and analysis of these applications are difficult, because the coupling mechanism is highly nonlinear and analytical solutions are not available in most cases[12]. A more effective approach is the simulation of behavior based on numerical method.

Several approximate numerical analysis methods have evolved over the years such as finite volume, finite difference, boundary element and finite element method. Finite difference method is, one of the most popular methods, used in various fields due to its efficiency. However, this method suffers from the drawback that it only provides a pointwise approximation of the solution[13]. This means when we encounter irregular geometries or an unusual specification of boundary conditions, finite difference method can not provide accurate solutions.

In engineering problems, finite element method(FEM), as the standard numerical calculation scheme for the computer simulation of physical systems, is most widely used, which has the advantages[14] of numerical efficiency, treatment of non-linearities, complex geometry, and analysis possibilities.

The question of accuracy and reliability of numerical solutions has led to the development of a large number of efficient and accurate error estimators in engineering mechanics. These error estimators are then employed to adaptively refine until a desired accuracy is reached. h-, p- and hp finite element methods are belonged to these estimators and can be used to simulate a number of problems accurately. Each finite element is characterized by its size h and order of approximation p. In the h-adaptive version of FEM, element size h may vary from element to element, while order of approximation p is fixed. In the p-adaptive version of the FEM, p may vary locally, while h remains constant throughout the adaptive procedure. Finally, a true hp-adaptive version of FEM allows for varying both h and p locally. The main motivation for the use of hp FEM is given by the following result[15]: an optimal sequence of hp-grids can achieve exponential convergence, whereas h- or p-FEM converge at best algebraically.

From previous discussions, we can find that it is of vital importance to investigate hp adaptive finite element method to simulate the coupled electrostatic mechanical behavior accurately, which is the goal of this thesis.

1.3 The Aim and Overview of the Thesis

1.3.1 The Aim of the Thesis

This thesis aims to generate a effective, efficient and robust hp adaptive finite element approach for two dimensional coupled electrostatic mechanical problem, in particular, for electrostriction. Generally, in the coupling between electrostatic and mechanical fields problems, the two domains overlap(totally or partially) and the coupling occurs through the differential governing equations describing the field quantities for electrostatics depend on mechanics and vice versa. In the electrostriction, the electrostatic force generated by electrostatic field will contribute to the volume force component of the differential governing equations in the mechanical field and the strains generated by mechanical field will effect the permittivity component in the electrostatic governing equations.

When we consider the nearly incompressible elastic materials, there is volumetric locking in the mechanical field, which can lead to incorrect results. It is then hoped that the hp adaptive finite element approach will be able to overcome locking and provide accurate results.

Using the method provided in the thesis, it is hoped small deformation electrostriction phenomenon can be simulated accurately. The success of this task will reveal the method can be extended to large deformation electrostriction, and further three dimensional coupling problems.

To achieve the aim, the task is divided into three main parts: electrostatic field simulation; mechanical field simulation; electrostriction simulation. The detailed work is described in the overview of the thesis.

1.3.2 Overview of the Thesis

This thesis is organized into five chapters as outlined below. The main body of the work is contained in Chapter 2 to 4, followed by the conclusion in Chapter 5.

Chapter 1: The background and numerical methods of the research are discussed which inspired this research issue. Furthermore, the aim and overview of the thesis are included.

Chapter 2: The mathematical theory and finite element formulation for the electrostatic field are discussed. The finite element method developed in MATLAB tested on a benchmark problem. Further, analytical solution for the benchmark problem is derived and convergence and accuracy of the method under h, p refinement is presented.

Chapter 3: The mathematical theory for linear elasticity is discussed followed by the displacement finite element formulation. Locking phenomena which can lead to inaccurate results is presented and mixed finite element formulation is derived to avoid locking. Furthermore, implementation of both displacement and mixed finite element methods is tested on a benchmark problem under h, p refinement in both plain strain and plain stress cases.

Chapter 4: The mathematical theory related to electrostriction is discussed. The methods for calculating electrostatic force are discussed also. Further, two algorithms with respect to one-way coupling and two-ways coupling are presented, respectively. Finally, results of the benchmark problem for both one-way coupling and two-ways coupling

are presented to show the effectiveness of the proposed hp adaptive finite element approach.

Chapter 5: This chapter discusses the summary, relevant conclusions of the thesis and some further research.

Chapter 2

Electrostatic Field

The full system of partial differential equations describing the electromagnetic field was published for the first time by James Clerk Maxwell in his work A Treatise on Electricity and Magnetism[16, 17] in the year 1862. He based his theory on the work and experiments of Ampere, Gauss, and Faraday. His great contribution lies in the unification of the different equations to a set of partial differential equations[14] which known as Maxwell's equations. For the static case, Maxwell's equations with constitutive laws can be separated into a magnetic and an electric subsystem. The electric subsystem is called the electrostatic case. In this chapter, electrostatic field problem is discussed without considering the effect from the mechanical field.

2.1 Mathematical Theory

For the electrostatic field, from Maxwell's equation, we obtain the following system of partial differential equations:

$$\boldsymbol{\nabla} \times \boldsymbol{E} = 0 \tag{2.1}$$

$$\boldsymbol{\nabla} \cdot \boldsymbol{D} = \rho_v \tag{2.2}$$

$$\boldsymbol{D} = \varepsilon \boldsymbol{E} \tag{2.3}$$

where E represents electric field intensity (V/m), D is electric flux density (As/m^2), ρ_v is charge density (As/m^3), and ε is electric permittivity (As/Vm).

Since the ***curl*** of the electric field intensity $\boldsymbol{E}$ is zero, we can express it by the gradient of a scalar potential Φ, which is called the electric scalar potential

$$\boldsymbol{E} = -\boldsymbol{\nabla}\Phi \tag{2.4}$$

. Thus, by combining (2.2), (2.3) and (2.4), we obtain:

$$-\boldsymbol{\nabla} \cdot \varepsilon \boldsymbol{\nabla}\Phi = \rho_v \tag{2.5}$$

. The electrostatic boundary value problem can be written as:

$$\boldsymbol{\nabla} \cdot (\varepsilon \nabla \Phi) = -\rho_v \qquad in\ \Omega \tag{2.6}$$

$$\Phi = f_D \qquad on\ \Gamma_D \tag{2.7}$$

$$\boldsymbol{n} \cdot (\varepsilon \boldsymbol{\nabla}\Phi) = f_N \qquad on\ \Gamma_N \tag{2.8}$$

As we know, there are two kinds of boundaries, Dirichlet boundary Γ_D where the potential value is defined and Neumann boundary Γ_N where the normal derivative of the potential is defined. In general, permittivity ε is a second order tensor. But for the problem considered in this chapter, we assume the domain consists of a linear, isotropic(but not necessarily homogeneous) medium. So ε is taken as a scalar function of position.

2.2 Finite Element Formulation

Let us consider the situation of a domain with given electric volume charges ρ_v, where we want to compute the generated electrostatic field.

The problem can be stated with (2.6, 2.7, 2.8). To obtain the weak form of the problem, we multiply (2.6) with an appropriate test function $w \in H_0^1$ and obtain:

$$\begin{aligned} \int_\Omega (\nabla \cdot (\epsilon \nabla \Phi)) w d\Omega &= -\int_\Omega \rho_v w d\Omega \qquad (2.9) \\ \int_\Omega \nabla \cdot (\epsilon \nabla \Phi w) d\Omega - \int_\Omega \epsilon \nabla \Phi \cdot \nabla w d\Omega &= -\int_\Omega \rho_v w d\Omega \end{aligned}$$

Here, $H^1(\Omega)$ is defined as:

$$u \in H^1(\Omega) \ : \ \int_\Omega |u|^2 + |\nabla u|^2 d\Omega < \infty \qquad (2.10)$$

Recall divergence theorem $\int_\Omega \nabla \cdot \boldsymbol{b} d\Omega = \int_\Gamma \boldsymbol{n} \cdot \boldsymbol{b} dS$ and $w = 0$ on Γ_D, the weak form reads as: Find $\Phi \in H_d^1$ such that

$$\int_\Omega \epsilon \nabla \phi \cdot \nabla w d\Omega = \int_{\Gamma_N} \boldsymbol{n} \cdot \epsilon \nabla \phi w dS + \int_\Omega \rho_v w d\Omega \qquad (2.11)$$

for any $w \in H_0^1$. An approximation to the electric scalar potential Φ as well as the test function w can be introduced as

$$\Phi = \sum_{i=1}^{m} \phi_i N_i \qquad (2.12)$$

$$w = \sum_{i=1}^{m} w_i N_i \qquad (2.13)$$

where ϕ_i are constant coefficients, N_i are shape functions and m represents the number of degrees of freedom. Therefore, the weak form is transformed into the following discrete formulation

$$\sum_{i=1}^{m} \sum_{j=1}^{m} (\int_\Omega \varepsilon (\nabla N_i)^T \nabla N_j d\Omega \phi_j - \int_\Omega N_i \rho_v d\Omega - \int \Gamma_N N_i \boldsymbol{n} \cdot (\varepsilon \nabla \phi) ds) = 0 \qquad (2.14)$$

In matrix form, it may be written as

$$\boldsymbol{K} \phi = \boldsymbol{r} \qquad (2.15)$$

where $\phi = (\phi_1, \phi_2, ..., \phi_m)^T$ and K, r are the global stiffness matrix and residual vector respectively, expressed as:

$$K = \sum_{e=1}^{E} k_{ij}^e; \quad k_{ij}^e = \int_{\Omega_e} (\varepsilon \nabla N_i \cdot \nabla N_j) d\Omega \tag{2.16}$$

$$r = \sum_{e=1}^{E} r_i^e; \quad r_i^e = \int_{\Omega} \rho_v N_i d\Omega + \int_{\Gamma_N} N_i \boldsymbol{n} \cdot (\varepsilon \nabla \phi) ds \tag{2.17}$$

where k_{ij}^e and r_i^e are elemental stiffness matrix and residual vector, respectively. E represents the number of elements in global mesh.

2.3 Higher Order Shape Functions

The domain is discretised into a set of non-overlapping triangular or quadrilateral elements. Usually the higher order shape functions are defined on reference elements and mapped to a general elements using a linear(bilinear) mapping. In the hp approach, the choice of the shape functions is different to the choice of the functions used for the mapping.

There are two common approaches to define higher order elements, which consist of the nodal approach and the hierarchic approach. In the nodal approach, the degrees of freedom corresponds to a specific solution at points within the element. Unfortunately, if the degree of element is increased, all shape functions must be replaced. In the hierarchic approach, the degrees of freedom do not correspond to the solution at a specific point, however, the existing shape functions are retained if the degree of the element is increased[18]. Therefore, the hierarchic shape functions are preferred in this thesis.

Schoberl and Zaglmayr[19, 20] have developed sets of triangular and quadrilateral finite element basis functions for the two dimensional

problem. In particular, to discretise the electrostatic finite element formulation, their basis functions for order p H^1 conforming elements are employed. A triangulation of Ω denoted by Γ_H is constructed using either quadrilaterals or triangles. The set of vertices is denoted by ν_H and the set of edges by ε_H. For the hierarchic scalar H^1 conforming finite element space a low order-vertex, high order edge-cell based splitting is adopted:

$$W_{h,p+1} := W_{h,1} \oplus \sum_{edges\ \ E \in \varepsilon_H} W^E_{p+1} \oplus \sum_{cells\ \ I \in \Gamma_H} W^I_{p+1} \subset H^1 \qquad (2.18)$$

The relevant basis functions for Schoberl and Zaglmayr's quadrilateral and triangular discretization can be found in [19, 20].

2.4 Computational Implementation

This section discusses issues related to computational implementation of the hp finite element formulation.

2.4.1 Evaluation of Elemental Integrals

In the same way as standard finite element shape functions, the previously defined shape functions are defined in a piecewise area, which means that when evaluating integrals such as k^e_{ij} or b^e_i, we only need to consider the set of shape functions associated with element e. However recall that shape functions N_i is defined in the reference element, whereas we need to integrate over the general physical element. To overcome this problem, a mapping between a physical element and a reference element is employed, denoted as Jacobian matrix J. J is expressed as:

$$J = \begin{pmatrix} \frac{\partial x}{\partial \hat{x}} & \frac{\partial x}{\partial \hat{y}} \\ \frac{\partial y}{\partial \hat{x}} & \frac{\partial y}{\partial \hat{y}} \end{pmatrix} \qquad (2.19)$$

where, x and y represent general coordinates whereas $\hat{x}$ and $\hat{y}$ are reference coordinates.

For shape functions, there is mapping as follows:

$$\nabla N = J^{-T}\hat{\nabla}N \tag{2.20}$$

In practice, most of these integrals is approximated by using Gauss quadrature[21].

2.4.2 Static Condensation

By numbering the degrees of freedom in a consistent manner, for example, grouping the all vertex functions, the all edge based functions, and the all interior functions. Denoting the group of vertex functions and edge based functions by C and the group of interior functions as I, then the linear equations system of structure can be expressed as:

$$\begin{pmatrix} K_{CC} & K_{CI} \\ K_{IC} & K_{II} \end{pmatrix} \begin{pmatrix} \phi_C \\ \phi_I \end{pmatrix} = \begin{pmatrix} r_C \\ r_I \end{pmatrix} \tag{2.21}$$

The interior degrees of freedom have no inter-element connectivity. Therefore, by using static condensation[22], it is possible to reduce the number of unknowns in the global system by eliminating the interior unknowns. Eliminating ϕ_I yields:

$$\tilde{K_{CC}}\phi_C = \tilde{b_C} \tag{2.22}$$

with

$$\tilde{K_{CC}} = K_{CC} - K_{CI}K_{II}^{-1}K_{IC} \tag{2.23}$$

$$\tilde{b_C} = b_C - K_{CI}K_{II}^{-1}b_I \tag{2.24}$$

Moreover, as K_{II} is block-diagonal this procedure can be applied during assembling so that:

$$\tilde{K_{CC}}^{e} = K_{CC}^{e} - K_{CI}^{e}K_{II}^{e-1}K_{IC}^{e} \tag{2.25}$$

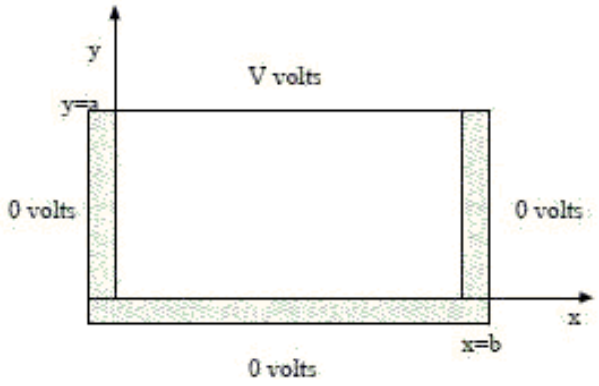

Figure 2.1: A conducting trough

$$\tilde{b_C}^e = b_C^e - K_{CI}^e K_{II}^{e-1} b_I^e \tag{2.26}$$

2.5 Benchmark Numerical Example

The electrostatic benchmark problem we discuss here is determining the potential for the region inside the rectangular trough of infinite length. The cross section of the trough and boundary conditions are shown in Figure(2.1). All the boundaries are Dirichlet boundaries and V=1. This problem has singularities in the corners and is chosen to discuss the convergence rate of hp refinement.

2.5.1 Analytical Solution

The permittivity ε is constant in the whole region and no variation in Z direction, so the governing equations for above problem can be expressed as:

$$\frac{\partial^2 \Phi}{\partial x^2} + \frac{\partial^2 \Phi}{\partial y^2} = 0 \tag{2.27}$$

The potential Φ can be divided into two parts using the technique of separation of variables,

$$\Phi = X(x)Y(y) \tag{2.28}$$

thus,

$$\begin{aligned} YX'' + XY'' &= 0 \\ -\frac{X''}{X} = \frac{Y''}{Y} &= \lambda \end{aligned} \tag{2.29}$$

where λ must be a constant, since it is a function of X only, and a function of Y only as well.

There are three cases, $\lambda = 0$, $\lambda < 0$, and $\lambda > 0$.

For the case $\lambda = 0$, then from (2.20), we can find X'' should be zero. Thus X can be expressed as:

$$X = Ax + B \tag{2.30}$$

Introducing boundary conditions $X(x = 0) = 0, X(x = b) = 0$, we can get:

$$X(x = 0) = B = 0 \tag{2.31}$$

$$X(x = b) = Ab = 0 \;\Rightarrow\; A = 0 \tag{2.32}$$

Thus X=0, which is incorrect. So $\lambda \neq 0$.

For the case $\lambda < 0$, say $\lambda = -\alpha^2$, then:

$$\frac{d^2X}{dx^2} - \alpha^2 X = 0 \tag{2.33}$$

Thus, the solution can be expressed as:

$$X = A_1 e^{\alpha x} + A_2 e^{-\alpha x} \tag{2.34}$$

Since,

$$\sinh \alpha x = \frac{e^{\alpha x} - e^{-\alpha x}}{2} \tag{2.35}$$

$$\cosh \alpha x = \frac{e^{\alpha x} + e^{-\alpha x}}{2} \tag{2.36}$$

then X can transform into:

$$X = B_1 \cosh \alpha x + B_2 \sinh \alpha x \tag{2.37}$$

with $B_1 = A_1 + A_2$ and $B_2 = A_1 - A_2$.

Introducing boundary conditions $X(x = 0) = 0, X(x = b) = 0$, we can get:

$$X(x = 0) = B_1 = 0 \tag{2.38}$$

$$X(x = b) = B_2 \sinh \alpha b = 0 \Rightarrow B_2 = 0 \tag{2.39}$$

Again, X=0, this case leads to incorrect solution.

So λ should be grater than zero and it can be written $\lambda = \alpha^2$. Then we can get:

$$\frac{d^2X}{dx^2} + \alpha^2 X = 0 \tag{2.40}$$

The solution of above equation can be expressed as:

$$X = A_1 \cos \alpha x + A_2 \sin \alpha x \tag{2.41}$$

Introducing boundary conditions $X(x = 0) = 0, X(x = b) = 0$, we can get $A_1 = 0, \sin \alpha b = 0$. α is expressed as:

$$\alpha = \frac{n\pi}{b}, n = 1, 2, 3, 4... \tag{2.42}$$

where the negative value of n would give rise to the same result as positive value, and when n=0, it leads to case 1, which gives incorrect solution, so n is considered as positive value here.

Thus λ is:

$$\lambda = \alpha^2 = \frac{n^2\pi^2}{b^2}, n = 1, 2, 3, 4... \tag{2.43}$$

The next step is to solve $Y'' - \lambda Y = 0$. Following the similar process as shown in above, we can get:

$$Y = B_n \sinh \frac{n\pi}{b} \tag{2.44}$$

Thus Φ_n can be written as:

$$\Phi_n = C_n \sin \frac{n\pi x}{b} \sinh \frac{n\pi y}{b} \tag{2.45}$$

The general solution of potential Φ can be given as:

$$\Phi = \sum_{n=1}^{\infty} C_n \sin \frac{n\pi x}{b} \sinh \frac{n\pi y}{b} \tag{2.46}$$

Introducing boundary condition $\Phi(x, a) = V$, then C_n can be obtained as:

$$C_n = \begin{cases} \frac{4V}{n\pi \sinh(n\pi a/b)} & n\ is\ odd \\ 0 & n\ is\ even \end{cases}$$

Finally, if we assume V=1, potential Φ can be expressed as:

$$\Phi = \frac{4}{\pi} \sum_{n=1,3,5...}^{\infty} \frac{\sin(\frac{n\pi x}{b}) \sinh(\frac{n\pi y}{b})}{n \sinh(\frac{n\pi a}{b})} \tag{2.47}$$

2.5.2 Numerical Results and Error Estimate

The numerical results of electrostatic potential are shown in Figure(2.2) and Figure(2.3). From these two figures, we can observe there are singularities near the top two corners of the domain.

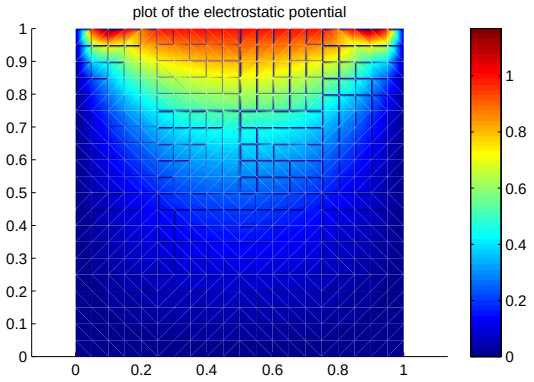

Figure 2.2: Contour plot of electrostatic potential

The analytical solution for this benchmark has been obtained in the

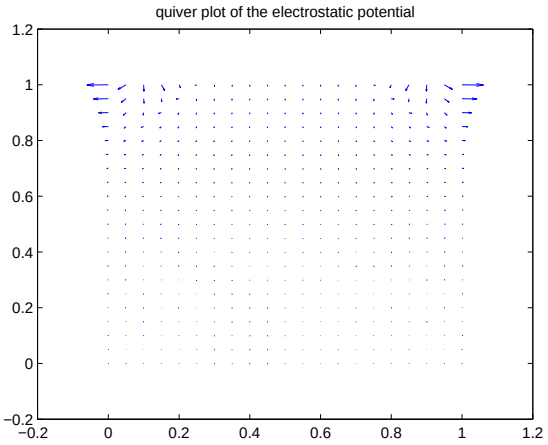

Figure 2.3: Quiver plot of electrostatic potential

previous section. Therefore, the magnitude of the error can be determined through comparing the finite element results with exact analytical solutions. Here, L_2 norm of the potential error is introduced to measure the error. It can be written as:

$$||e_\Phi||_{L_2} = [\int_\Omega (\Phi - \Phi_{hp})^2 d\Omega]^{1/2} \tag{2.48}$$

where Φ_{hp} represents the numerical solution obtained from the finite element method.

Figure(2.4) and Figure(2.5) shows L_2 norm of the potential error with h and p refinement, respectively, where x axis represents log(number of degrees of freedom) and y axis is log(L_2 norm of potential error). From the two figures, we can conclude the error converges algebraically fast with both h, p refinements as expected. Because there are singularities in top two corners, only algebraic convergence rate can be observed with uniform h or p refinement. However, if the domain has smooth solution, then p refinement may present exponential convergence rate. With general case, appropriate combination of h,p refinement (hp FEM) will lead to exponential convergence rate. If we want

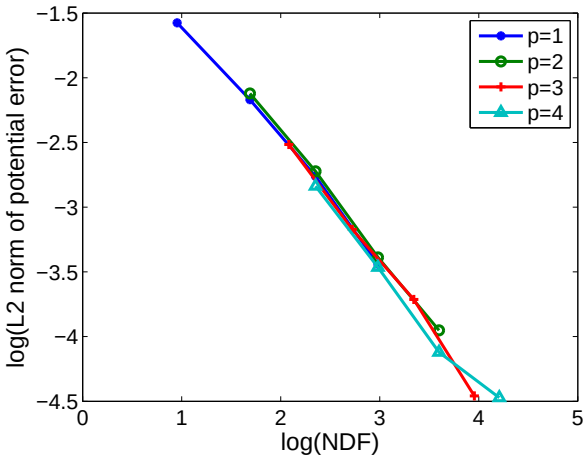

Figure 2.4: L2 norm of the potential error with h refinement

to obtain exponential convergence rate for this benchmark which has singularities, we need to combine h and p refinement. That means instead of uniform mesh, we can use nonuniform mesh in Figure(2.6) to refine the two corners which have singularities more properly. The combination of these kinds of nonuniform mesh and p refinement may obtain exponential convergence rate. But due to time constraint, we haven't obtained the results with exponential convergence rate. This can be considered and tried in future work.

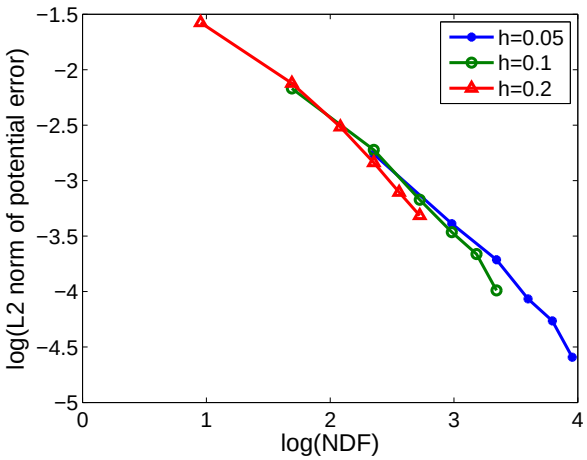

Figure 2.5: L2 norm of the potential error with p refinement

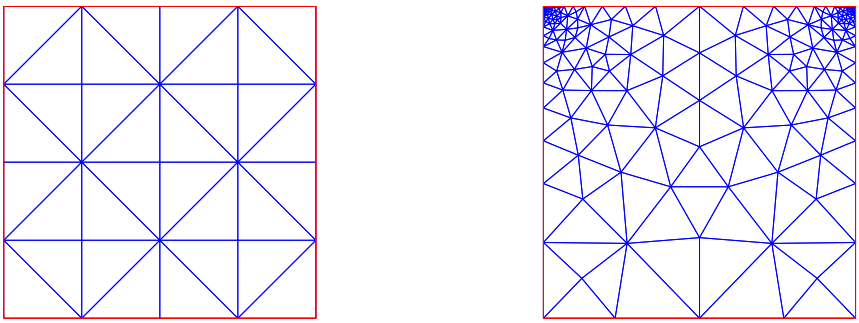

Figure 2.6: Uniform mesh and specified nonuniform mesh

Chapter 3

Mechanical Field

3.1 Mathematical Theory

The elastostatic boundary value problem can be written as

$$\begin{aligned} \nabla \cdot \boldsymbol{\sigma} + \boldsymbol{f} &= \mathbf{0} \qquad in\Omega \\ \boldsymbol{u} &= \boldsymbol{u_D} \qquad on\Gamma_D \\ \boldsymbol{\sigma} \cdot \boldsymbol{n} &= \boldsymbol{t_N} \qquad on\Gamma_N \end{aligned} \tag{3.1}$$

This partial differential equation system represents "translational equilibrium", in which $\boldsymbol{\sigma}$ represents the Cauchy stress tensor, $\boldsymbol{f}$ is body force vector, $\boldsymbol{u}$ is displacement vector and $\boldsymbol{t}$ is the traction vector. The displacement value is defined on Dirichlet boundary and the traction is defined on the Neumann boundary.
Recall that strain tensor $\boldsymbol{\epsilon}$ can be expressed as

$$\boldsymbol{\epsilon} = \frac{1}{2}(\nabla \boldsymbol{u} + \nabla \boldsymbol{u^T}) \tag{3.2}$$

Recall also that "rotational equilibrium" yields $\boldsymbol{\sigma} = \boldsymbol{\sigma^T}$. In order to close the system, an equation of state (so called "constitutive equation") must also be added. This equation which will relate $\boldsymbol{\sigma}$ with $\boldsymbol{\epsilon}$ is

expressed as

$$\boldsymbol{\sigma} = \boldsymbol{c} : \boldsymbol{\epsilon} \tag{3.3}$$

where $\boldsymbol{c}$ is the fourth order constitutive elasticity tensor.
The simplest hyperelastic material–St. Venant–Kirchhoff model can be defined by a strain energy function Ψ as

$$\Psi(\boldsymbol{\epsilon}) = \frac{\lambda}{2}(\mathrm{I}_{\boldsymbol{\epsilon}})^2 + \mu \mathrm{II}_{\boldsymbol{\epsilon}} \tag{3.4}$$

where invariants $\mathrm{I}_{\boldsymbol{\epsilon}} = tr(\boldsymbol{\epsilon})$ and $\mathrm{II}_{\boldsymbol{\epsilon}} = \boldsymbol{\epsilon} : \boldsymbol{\epsilon}$. λ and μ are so called Lame constants, and expressed in terms of the Poisson ratio(ν) and Young's modulus(E) as:

$$\lambda = \frac{E\nu}{(1+\nu)(1-2\nu)} \tag{3.5}$$

$$\mu = \frac{E}{2(1+\nu)} \tag{3.6}$$

There are two cases in two dimensional mechanical problems. One is plain strain case, the other is plain stress case.
The plain strain case is a simplification of the general case and can be used when the third dimension(assumed as the z-direction) is very large and within each cross section the same boundary conditions as well as forces act on the body[14]. Therefore, $\boldsymbol{\epsilon_{33}} = \boldsymbol{\epsilon_{23}} = \boldsymbol{\epsilon_{13}} = \boldsymbol{\epsilon_{31}} = \boldsymbol{\epsilon_{32}} = \mathbf{0}$. Thus, the strain energy function is transformed into:

$$\Psi(\boldsymbol{\epsilon_{2\times 2}}) = \frac{\lambda}{2}(\mathrm{I}_{\boldsymbol{\epsilon_{2\times 2}}})^2 + \mu \mathrm{II}_{\boldsymbol{\epsilon_{2\times 2}}} \tag{3.7}$$

where,

$$\boldsymbol{\epsilon} = \begin{pmatrix} \epsilon_{11} & \epsilon_{12} & 0 \\ \epsilon_{21} & \epsilon_{22} & 0 \\ 0 & 0 & 0 \end{pmatrix}, \qquad \boldsymbol{\epsilon_{2\times 2}} = \begin{pmatrix} \epsilon_{11} & \epsilon_{12} \\ \epsilon_{21} & \epsilon_{22} \end{pmatrix} \tag{3.8}$$

The plain stress case can be used when a thin sheet is loaded by mechanical forces at the boundary and the forces act within the defined

plane[14]. Therefore, $\boldsymbol{\sigma_{33} = \sigma_{23} = \sigma_{13} = \sigma_{31} = \sigma_{32} = 0}$. Thus, the strain energy function is transformed into:

$$\Psi(\boldsymbol{\epsilon_{2\times 2}}) = \frac{\hat{\lambda}}{2}(\mathrm{I}_{\boldsymbol{\epsilon_{2\times 2}}})^2 + \mu \mathrm{II}_{\boldsymbol{\epsilon_{2\times 2}}} \tag{3.9}$$

where,

$$\hat{\lambda} = \frac{2\lambda\mu}{\lambda + 2\mu} \tag{3.10}$$

For a hyperelastic material, the Cauchy stress tensor $\boldsymbol{\sigma}$ can be deduced from:

$$\boldsymbol{\sigma} = \frac{\partial \Psi}{\partial \boldsymbol{\epsilon}} \tag{3.11}$$

Thus the Cauchy stress tensor can be written as:

$$\boldsymbol{\sigma_{2\times 2}} = \tilde{\lambda}\mathrm{I}_{\boldsymbol{\epsilon_{2\times 2}}}\mathbf{I} + 2\mu\boldsymbol{\epsilon_{2\times 2}} \tag{3.12}$$

where $\tilde{\lambda} = \lambda$ for plain strain case and $\tilde{\lambda} = \hat{\lambda}$ for plain stress case.
In this case, the constitutive elasticity tensor is given as

$$\boldsymbol{c} = \frac{\partial \boldsymbol{\sigma_{2\times 2}}}{\partial \boldsymbol{\epsilon_{2\times 2}}} = \tilde{\lambda}\mathbf{I} \otimes \mathbf{I} + 2\mu\boldsymbol{i} \tag{3.13}$$

where $\boldsymbol{i}$ is the fourth-order identity tensor. That means for any second order tensor $\boldsymbol{s}$, it satisfies $\boldsymbol{i} : \boldsymbol{s} = \boldsymbol{s}$.

3.2 Displacement Finite Element Formulation

The strong form of the linear elastostatic problems is written as (3.1), where we want to compute the displacement field $\boldsymbol{u}$. In the small strain linear elasticity considered in this chapter, the principle of virtual work can be derived by finding the stationary position of a total energy potential.
A total potential energy functional can be defined as:[23]

$$\Pi(\boldsymbol{\phi}) = \int_\Omega \Psi d\Omega - \int_\Omega \boldsymbol{f} \cdot \boldsymbol{\phi} d\Omega - \int_{\Gamma_N} \boldsymbol{t} \cdot \boldsymbol{\phi} d\Gamma \tag{3.14}$$

Equating the derivative of the functional to zero in an arbitrary direction $\delta\boldsymbol{u}$ gives the stationary position. This means the principle virtual work is obtained as

$$\delta W(\boldsymbol{\phi}, \delta\boldsymbol{u}) = D\Pi(\boldsymbol{\phi})[\delta\boldsymbol{u}] = \int_\Omega \boldsymbol{\sigma} : \delta\boldsymbol{\epsilon} d\Omega - \int_\Omega \boldsymbol{f} \cdot \delta\boldsymbol{u} d\Omega - \int_{\Gamma_N} \boldsymbol{t} \cdot \delta\boldsymbol{u} d\Gamma \tag{3.15}$$

where,

$$\delta W_{int}(\boldsymbol{\phi}, \delta\boldsymbol{u}) = \int_\Omega \boldsymbol{\sigma} : \delta\boldsymbol{\epsilon} d\Omega \tag{3.16}$$

$$\delta W_{ext}(\boldsymbol{\phi}, \delta\boldsymbol{u}) = \int_\Omega \boldsymbol{f} \cdot \delta\boldsymbol{u} d\Omega + \int_{\Gamma_N} \boldsymbol{t} \cdot \delta\boldsymbol{u} d\Gamma \tag{3.17}$$

Linearized principle of virtual work with respect to a displacement field $\boldsymbol{u}$ renders

$$D\delta W(\boldsymbol{\phi}, \delta\boldsymbol{u})[\boldsymbol{u}] = D\delta W_{int}(\boldsymbol{\phi}, \delta\boldsymbol{u})[\boldsymbol{u}] - D\delta W_{ext}(\boldsymbol{\phi}, \delta\boldsymbol{u})[\boldsymbol{u}] = 0 \tag{3.18}$$

Linearized the internal virtual work renders:

$$D\delta W_{int}(\boldsymbol{\phi}, \delta\boldsymbol{u})[\boldsymbol{u}] = D(\int_\Omega \boldsymbol{\sigma} : \delta\boldsymbol{\epsilon} d\Omega)[\boldsymbol{u}] = \int_\Omega (\delta\boldsymbol{\epsilon} : \boldsymbol{c} : \boldsymbol{\epsilon}) d\Omega \tag{3.19}$$

On the other hand, linearized external virtual work renders:

$$D\delta W_{ext}(\boldsymbol{\phi}, \delta\boldsymbol{u})[\boldsymbol{u}] D\delta W_{int}(\boldsymbol{\phi}, \delta\boldsymbol{u})[\boldsymbol{u}] = D(\int_\Omega \boldsymbol{f} \cdot \delta\boldsymbol{u} d\Omega + \int_{\Gamma_N} \boldsymbol{t} \cdot \delta\boldsymbol{u} d\Gamma)[\boldsymbol{u}] = 0 \tag{3.20}$$

Thus:

$$\delta W(\boldsymbol{\phi}, \delta\boldsymbol{u}) + D\delta W(\boldsymbol{\phi}, \delta\boldsymbol{u})[\boldsymbol{u}] = 0 \tag{3.21}$$

which when discretized yields,

$$\boldsymbol{R} + \boldsymbol{K}\boldsymbol{u} = 0 \tag{3.22}$$

where, $\boldsymbol{K}$ is stiffness matrix and -$\boldsymbol{R}$ is residual vector.

The unknown displacement field $\boldsymbol{u}$ can be approximated in terms of a

series of shape functions as

$$\boldsymbol{u} \approx \boldsymbol{u}^h = \sum_{a=1}^{m} N_a \boldsymbol{u}_a \tag{3.23}$$

$$\delta\boldsymbol{u} \approx \delta\boldsymbol{u}^h = \sum_{a=1}^{m} N_a \delta\boldsymbol{u}_a \tag{3.24}$$

The virtual work expression can be expended for an element (e) as:

$$\begin{aligned} \delta W^e(\boldsymbol{\phi}, N_a\delta\boldsymbol{u}_a) &= \delta\boldsymbol{u}_a \cdot \int_{\Omega_e} \boldsymbol{\sigma}\nabla N_a d\Omega \\ &- \delta\boldsymbol{u}_a \cdot [\int_{\Omega_e} N_a \boldsymbol{f} d\Omega + \int_{\Gamma_{N(e)}} N_a \boldsymbol{t} d\Gamma] = 0 \end{aligned} \tag{3.25}$$

or equivalently,

$$\delta W^e(\boldsymbol{\phi}, N_a\delta\boldsymbol{u}_a) = \delta\boldsymbol{u}_a \cdot (\boldsymbol{T}_a^e - \boldsymbol{F}_a^e) = 0 \tag{3.26}$$

where, $\boldsymbol{T}_a^e$ and $\boldsymbol{F}_a^e$ are equivalent internal force and external force, respectively, and is written as:

$$\boldsymbol{T}_a^e = \int_{\Omega_e} \boldsymbol{\sigma}\nabla N_a d\Omega \tag{3.27}$$

$$\boldsymbol{F}_a^e = \int_{\Omega_e} N_a \boldsymbol{f} d\Omega + \int_{\Gamma_{N(e)}} N_a \boldsymbol{t} d\Gamma \tag{3.28}$$

Therefore, the elemental residual force vector r_a^e is equal to -$\boldsymbol{R}_a^e$ and can be expressed as:

$$r_a^e = \boldsymbol{F}_a^e - \boldsymbol{T}_a^e \tag{3.29}$$

Analogously, the linearized virtual work expression renders for an element (e):

$$\begin{aligned} D\delta W(\boldsymbol{\phi}, N_a\delta\boldsymbol{u}_a)[N_b\boldsymbol{u}_b] &= \int_{\Omega_e} \delta\boldsymbol{\epsilon} : \boldsymbol{c} : \boldsymbol{\epsilon} d\Omega \\ = \int_{\Omega_e} (\delta\boldsymbol{u}_a \otimes \nabla N_a) &: \boldsymbol{c}^{sym} : (\nabla N_b \otimes \boldsymbol{u}_b) d\Omega \end{aligned} \tag{3.30}$$

or in index notation, above equation can be expressed as:

$$\begin{aligned} \delta u_a(i)[\int_{\Omega_e} \sum_{k,l=1}^{2} \frac{\partial N_a}{\partial x_k} \boldsymbol{c}_{ikjl}^{sym} \frac{\partial N_b}{\partial x_l} d\Omega] u_b(j); \qquad i,j = 1,2 \\ = \delta u_a(i)[[K_{ab}]_{ij}^e] u_b(j) \end{aligned} \tag{3.31}$$

Here, $[K_{ab}]^e_{ij}$ is elemental constitutive stiffness matrix,and has the following expression:

$$[K_{ab}]^e_{ij} = \int_{\Omega_e} \sum_{k,l=1}^{2} \frac{\partial N_a}{\partial x_k} \boldsymbol{c}^{sym}_{ikjl} \frac{\partial N_b}{\partial x_l} d\Omega; \qquad i,j = 1,2 \tag{3.32}$$

After suitable assemble of the elemental constitutive stiffness matrix and elemental residual force vectors, we can obtain a linear system of equations:

$$K\boldsymbol{U} = \boldsymbol{r} \tag{3.33}$$

where $\boldsymbol{U} = (\boldsymbol{u}_1, \boldsymbol{u}_2, ..., \boldsymbol{u}_m)$, K is the global stiffness matrix and r is the residual force vector. K and r are the assemblage of elemental stiffness matrix and residual vectors, respectively.

$$K = \sum_{e=1}^{E} K^e_{ab} \tag{3.34}$$

$$r = \sum_{e=1}^{E} r^e_a \tag{3.35}$$

where E represents the number of elements in global mesh.
For displacement formulation, the same shape functions as used in electrostatic field are also used here.

3.3 Locking and Efficient Solution Approaches

3.3.1 Locking Phenomena

For many problems in computational mechanics, various quantities of engineering interest like displacements and stresses can be accurately calculated by using the displacement finite element formulation. However, for some problems, displacement finite element method will provide inaccurate results and show slow convergence when reducing mesh size. We will refer to this effect as locking. In general, there are

three main locking phenomena and they are shear locking, volumetric(Poisson) locking, and membrane locking. In this thesis, we will concentrate on the volumetric locking. For nearly incompressible materials(Poisson ratio ν close to 0.5, which means Lame constant λ close to ∞), displacement based finite element method can lead to volumetric locking[14]. Then displacements and stresses may be computed inaccurately[24]. Next, we start with a mathematical investigation of the volumetric locking[25]. Recall that the expression of strain tensor:

$$\boldsymbol{\epsilon} = \frac{1}{2}(\nabla \boldsymbol{u} + \nabla \boldsymbol{u}^T) \tag{3.36}$$

The volumetric strain is defined as the trace of the strain tensor as:

$$\epsilon_v = tr(\boldsymbol{\epsilon}) = I_{\boldsymbol{\epsilon}} = div(\boldsymbol{u}) \tag{3.37}$$

Thus the strain can be additively decomposed into their deviatoric and volumetric components as follows:

$$\boldsymbol{\epsilon} = \boldsymbol{\epsilon}^{'} + \frac{1}{3}tr(\boldsymbol{\epsilon})\boldsymbol{I} = \boldsymbol{\epsilon}^{'} + \frac{1}{3}div(\boldsymbol{u})\boldsymbol{I} \tag{3.38}$$

where, the former term is deviatoric component and the latter one is volumetric component.

Analogously, the stress tensor can also be decomposed as:

$$\boldsymbol{\sigma} = \boldsymbol{\sigma}^{'} + P\boldsymbol{I} \tag{3.39}$$

where, the former term is deviatoric component and the latter one is volumetric component. Here, $p = \frac{1}{3}tr(\boldsymbol{\sigma})$ is the so-called hydrostatic pressure.

For a standard linear elastic model, the stress tensor is:

$$\boldsymbol{\sigma} = \lambda tr(\boldsymbol{\epsilon})\boldsymbol{I} + 2\mu\boldsymbol{\epsilon} \tag{3.40}$$

Substituting $\boldsymbol{\epsilon}$ with (3.38), stress can be written as:

$$\boldsymbol{\sigma} = [\lambda + \frac{2\mu}{3}]tr(\boldsymbol{\epsilon})\boldsymbol{I} + 2\mu\boldsymbol{\epsilon}^{'} \tag{3.41}$$

where, the first term is volumetric component and the second one is deviatoric component.

Introducing bulk modulus k,

$$k = \lambda + \frac{2\mu}{3} = \frac{E}{3(1-2\nu)} \tag{3.42}$$

then $\boldsymbol{\sigma} = P\boldsymbol{I} + \boldsymbol{\sigma}^{'}$, where

$$\begin{aligned} \boldsymbol{\sigma}^{'} &= 2\mu\boldsymbol{\epsilon}^{'} && (3.43) \\ P &= k\ tr(\boldsymbol{\epsilon}) = k\ div(\boldsymbol{u}) && (3.44) \end{aligned}$$

Here, k can be also understand as a penalty term, introduced with a purpose of satisfying incompressibility.

Thus, as $k \to \infty$ ($\nu \to 0.5$), the problem becomes ill-conditioned and volumetric locking occurs.

It's been demonstrated as below.

Recall internal virtual work from formula,

$$\delta W_{int}(\boldsymbol{\phi}, \delta\boldsymbol{u}) = \int_{\Omega} \boldsymbol{\sigma} : \delta\boldsymbol{\epsilon} d\Omega \tag{3.45}$$

Notice that:

$$\begin{aligned} \boldsymbol{\sigma} : \delta\boldsymbol{\epsilon} &= (\boldsymbol{\sigma}^{'} + P\boldsymbol{I}) : (\delta\boldsymbol{\epsilon}^{'} + \frac{1}{3} div(\delta\boldsymbol{u})\boldsymbol{I}) \\ &= \boldsymbol{\sigma}^{'} : \delta\boldsymbol{\epsilon}^{'} + P\ div(\delta\boldsymbol{u}) && (3.46) \end{aligned}$$

Thus, internal virtual work form is transformed into:

$$\delta W_{int}(\boldsymbol{\phi}, \delta\boldsymbol{u}) = \int_{\Omega} \boldsymbol{\sigma}^{'} : \delta\boldsymbol{\epsilon}^{'} d\Omega + \int_{\Omega} P\ div(\delta\boldsymbol{u}) d\Omega \tag{3.47}$$

where the first term is deviatoric internal virtual work defined as $\delta W_{int}^{'}(\boldsymbol{\phi}, \delta\boldsymbol{u})$, and the second term is volumetric internal virtual work defined as $\delta W_{int}^{P}(\boldsymbol{\phi}, \delta\boldsymbol{u})$.

After applying the constitutive relationship $P = k\ div(\boldsymbol{u})$, the volumetric component of the internal virtual work renders:

$$\delta W_{int}^{P}(\boldsymbol{\phi}, \delta\boldsymbol{u}) = \int_{\Omega} k\ div(\boldsymbol{u}) div(\delta\boldsymbol{u}) d\Omega \tag{3.48}$$

Again, as k grows ($k \rightarrow \infty$), $\delta W_{int}^{P}(\boldsymbol{\phi}, \delta \boldsymbol{u})$ locks the problem.
Therefore, we will:

- Define a constitutive equation which is only a function of the distortional component of the deformation, $\Psi^{'}(\boldsymbol{\epsilon}) = \Psi(\boldsymbol{\epsilon}^{'})$
- Enforce explicitly the incompressibility constraint $div(\boldsymbol{u}) = 0$

3.3.2 Efficient Solution Approaches

hp FEM is one of the efficient approaches to avoid locking. As discussed in the previous chapter, solution with required accuracy can be achieved by proper combination of h and p refinement. There are also other approaches discussed in the book[23]. Among them, HU-WASHIZU principle is one of efficient solutions to deal with locking problem. Further, mixed finite element formulation will be derived based on this principle. The objective of this principle is to minimize the total potential energy functional defined as following expression:

$$\Pi_{HW}(\boldsymbol{\phi}, \bar{\boldsymbol{\epsilon}_{\boldsymbol{v}}}, P) = \int_{\Omega} \Psi^{'}(\boldsymbol{\epsilon}) d\Omega + \int_{\Omega} U(\bar{\boldsymbol{\epsilon}_{\boldsymbol{v}}}) d\Omega + \int_{\Omega} P(\boldsymbol{\epsilon}_{\boldsymbol{v}} - \bar{\boldsymbol{\epsilon}_{\boldsymbol{v}}}) d\Omega - \Pi_{ext}(\boldsymbol{\phi}) \tag{3.49}$$

where, $\Psi^{'}(\boldsymbol{\epsilon})$ represents deviatoric energy, $U(\bar{\boldsymbol{\epsilon}_{\boldsymbol{v}}})$ represents volumetric energy, and $\boldsymbol{\epsilon}_{\boldsymbol{v}} = div(\boldsymbol{u})$.
$U(\bar{\boldsymbol{\epsilon}_{\boldsymbol{v}}})$ can be expressed as:

$$U(\bar{\boldsymbol{\epsilon}_{\boldsymbol{v}}}) = \frac{k}{2}(\bar{\boldsymbol{\epsilon}_{\boldsymbol{v}}})^2 \tag{3.50}$$

Other functions U might be used.
$\bar{\boldsymbol{\epsilon}_{\boldsymbol{v}}}$ and P are independent of the motion defined by $\boldsymbol{\phi}$, that means:

$$\bar{\boldsymbol{\epsilon}_{\boldsymbol{v}}} \neq div(\boldsymbol{u}) \tag{3.51}$$

$$p \neq (\lambda + \frac{2}{3}\mu) div(\boldsymbol{u}) \tag{3.52}$$

The stationary point of above energy functional yields:

$$\begin{aligned} D\Pi_{HW}(\boldsymbol{\phi}, \bar{\boldsymbol{\epsilon_v}}, P)[\delta\boldsymbol{u}] &= \int_\Omega \frac{\partial \Psi^{'}}{\partial \boldsymbol{\epsilon}} : \delta\boldsymbol{\epsilon} d\Omega + \int_\Omega P div(\delta\boldsymbol{u}) d\Omega \\ &- D\Pi_{ext}(\boldsymbol{\phi})[\delta\boldsymbol{u}] = 0 \qquad (3.53) \\ D\Pi_{HW}(\boldsymbol{\phi}, \bar{\boldsymbol{\epsilon_v}}, P)[\delta\bar{\boldsymbol{\epsilon_v}}] &= \int_\Omega (\frac{dU(\bar{\boldsymbol{\epsilon_v}})}{d\bar{\boldsymbol{\epsilon_v}}} - P)\delta\bar{\boldsymbol{\epsilon_v}} d\Omega = 0 \qquad (3.54) \\ D\Pi_{HW}(\boldsymbol{\phi}, \bar{\boldsymbol{\epsilon_v}}, P)[\delta P] &= \int_\Omega (\boldsymbol{\epsilon_v} - \bar{\boldsymbol{\epsilon_v}})\delta P d\Omega = 0 \qquad (3.55) \end{aligned}$$

Let's assume that P, $\bar{\boldsymbol{\epsilon_v}}$ (and thus δP, $\delta\bar{\boldsymbol{\epsilon_v}}$) are function which remain constant within the domain Ω, thus:

From(3.54), we can obtain:

$$(\frac{dU(\bar{\boldsymbol{\epsilon_v}})}{d\bar{\boldsymbol{\epsilon_v}}} - P)\delta\bar{\boldsymbol{\epsilon_v}}\Omega = 0 \;\Rightarrow\; P = \frac{dU(\bar{\boldsymbol{\epsilon_v}})}{d\bar{\boldsymbol{\epsilon_v}}} = k\bar{\boldsymbol{\epsilon_v}} \qquad (3.56)$$

From(3.55), we can obtain:

$$[\int_\Omega \boldsymbol{\epsilon_v} d\Omega - \bar{\boldsymbol{\epsilon_v}}\Omega]\delta P = 0 \;\Rightarrow\; \bar{\boldsymbol{\epsilon_v}} = \frac{\int_\Omega \boldsymbol{\epsilon_v} d\Omega}{\Omega} \qquad (3.57)$$

Thus:

$$\begin{aligned} \bar{\boldsymbol{\epsilon_v}} &= \frac{1}{\Omega}\int_\Omega div(\boldsymbol{u}) d\Omega \qquad (3.58) \\ P &= k\bar{\boldsymbol{\epsilon_v}} = \frac{k}{\Omega}\int_\Omega div(\boldsymbol{u}) d\Omega \qquad (3.59) \end{aligned}$$

Recall that:

$$\boldsymbol{\sigma} = \boldsymbol{\sigma}^{'} + p\boldsymbol{I} \qquad (3.60)$$

where

$$\boldsymbol{\sigma}^{'} = \frac{\partial \Psi^{'}}{\partial \boldsymbol{\epsilon}} = 2\mu\boldsymbol{\epsilon}^{'} \qquad (3.61)$$

and P is stated above.

Constitutive tensor $\boldsymbol{c}$ is now replaced by $\boldsymbol{c}^{'}$ and can be deduced from:

$$\boldsymbol{c}^{'} = \frac{\partial^2 \Psi^{'}}{\partial\boldsymbol{\epsilon}\partial\boldsymbol{\epsilon}} = \frac{\partial\boldsymbol{\sigma}^{'}}{\partial\boldsymbol{\epsilon}} \qquad (3.62)$$

We can deduce for the plain strain case and plain stress case as:
In plane strain case:

$$
\begin{aligned}
k &= \lambda + \mu && (3.63)\\
\boldsymbol{\sigma}^{'}_{2\times 2} &= 2\mu\boldsymbol{\epsilon}_{2\times 2} - \mu\ tr(\boldsymbol{\epsilon}_{2\times 2})\boldsymbol{I_{2\times 2}} && (3.64)\\
\boldsymbol{c}^{'} &= \frac{\partial \boldsymbol{\sigma}^{'}_{2\times 2}}{\partial \boldsymbol{\epsilon}_{2\times 2}} && (3.65)\\
\boldsymbol{c}^{sym}_{ijkl} &= \mu(\delta_{ik}\delta jl + \delta jk\delta il) - \mu\delta_{ij}\delta_{kl} && (3.66)
\end{aligned}
$$

In plane stress case:

$$
\begin{aligned}
k &= (\mu + \frac{3}{2}\lambda)\frac{2\mu}{\lambda + 2\mu} && (3.67)\\
\boldsymbol{\sigma}^{'}_{2\times 2} &= 2\mu\boldsymbol{\epsilon}_{2\times 2} - \mu\ tr(\boldsymbol{\epsilon}_{2\times 2})\boldsymbol{I_{2\times 2}} && (3.68)\\
\boldsymbol{c}^{'} &= \frac{\partial \boldsymbol{\sigma}^{'}_{2\times 2}}{\partial \boldsymbol{\epsilon}_{2\times 2}} && (3.69)\\
\boldsymbol{c}^{sym}_{ijkl} &= \mu(\delta_{ik}\delta jl + \delta jk\delta il) - \mu\delta_{ij}\delta_{kl} && (3.70)
\end{aligned}
$$

3.4 Mixed Finite Element Formulation

Now, we describe the mixed formulation which based on HU-WASHIZU principle. A modified total potential energy functional can be defined as:

$$\Pi(\boldsymbol{\phi}, p) = \int_\Omega \Phi^{'} d\Omega + \int_\Omega p div(\boldsymbol{u}) d\Omega - \int_\Omega \frac{p^2}{2k} d\Omega - \Pi_{ext}(\boldsymbol{\phi}) \qquad (3.71)$$

where $\Pi_{ext} = \int_\Omega \boldsymbol{f}\cdot\boldsymbol{\phi} d\Omega + \int_{\Gamma_N} \boldsymbol{t}\cdot\boldsymbol{\phi} d\Gamma$.
The stationary point of above functional yields:

$$
\begin{aligned}
D\Pi(\boldsymbol{\phi}, p)[\delta\boldsymbol{u}] &= \int_\Omega \frac{\delta\Phi^{'}}{\delta\boldsymbol{\epsilon}} : \delta\boldsymbol{\epsilon} d\Omega + \int_\Omega p div(\delta\boldsymbol{u}) d\Omega - D\Pi_{ext}(\phi)[\delta\boldsymbol{u}] && (3.72)\\
D\Pi(\boldsymbol{\phi}, p)[\delta p] &= \int_\Omega \delta p div(\boldsymbol{u}) d\Omega - \int_\Omega \delta p \frac{p}{k} d\Omega\\
&= \int_\Omega \delta p (div(\boldsymbol{u}) - \frac{p}{k}) d\Omega && (3.73)
\end{aligned}
$$

Linearizing above two equations respect to $\boldsymbol{u}$ and p will yield:

$$D^2\Pi(\boldsymbol{\phi},p)[\delta\boldsymbol{u}][\boldsymbol{u}] = \int_\Omega \delta\boldsymbol{\epsilon} : \frac{\partial\boldsymbol{\sigma}'}{\partial\boldsymbol{\epsilon}} : \boldsymbol{\epsilon} d\Omega \tag{3.74}$$

$$D^2\Pi(\boldsymbol{\phi},p)[\delta\boldsymbol{u}][p] = \int_\Omega div(\delta\boldsymbol{u}) p d\Omega \tag{3.75}$$

$$D^2\Pi(\boldsymbol{\phi},p)[\delta p][\boldsymbol{u}] = \int_\Omega \delta p div(\boldsymbol{u}) d\Omega \tag{3.76}$$

$$D^2\Pi(\boldsymbol{\phi},p)[\delta p][p] = -\frac{1}{k}\int_\Omega \delta p\ p d\Omega \tag{3.77}$$

The unknown displacement field $\boldsymbol{u}$ and p can be expressed in terms of a series of shape functions respectively as:

$$\boldsymbol{u} = \sum_{a=1}^{N} N_u^a \boldsymbol{u}^a, \qquad p = \sum_{a=1}^{N} N_p^a p^a \tag{3.78}$$

For an element Ω_e, the elemental stiffness component and residual matrices are expressed as:

$$[K^e_{c',ab}]_{ij} = \int_{\Omega_e} \sum_{k,l=1}^{2} \frac{\partial N_u^a}{\partial x_k} \boldsymbol{c}'^{sym}_{ikjl} \frac{\partial N_u^b}{\partial x_l} d\Omega; \qquad i,j = 1,2 \tag{3.79}$$

$$K^e_{up,ab} = \int_{\Omega_e} \nabla N_u^a N_p^b d\Omega \tag{3.80}$$

$$K^e_{pu,ab} = \int_{\Omega_e} N_p^a (\nabla N_u^b)^T d\Omega \tag{3.81}$$

$$K^e_{pp,ab} = -\frac{1}{k}\int_{\Omega_e} N_p^a N_p^b d\Omega \tag{3.82}$$

$$\boldsymbol{r}_a^e = \int_{\Omega_e} N_a \boldsymbol{f} d\Omega + \int_{\Gamma_e} N_a \boldsymbol{t} ds - \int_{\Omega_e} \boldsymbol{\sigma} \nabla N_a d\Omega \tag{3.83}$$

This will lead to the following system of equations on the element level:

$$\begin{pmatrix} K^e_{c'} & K^e_{up} \\ K^e_{pu} & K^e_{pp} \end{pmatrix} \begin{pmatrix} \boldsymbol{u} \\ p \end{pmatrix} = \begin{pmatrix} \boldsymbol{r}^e \\ 0 \end{pmatrix} \tag{3.84}$$

If shape functions N_p^a are chosen such that static condensation can be performed, then according to the static condensation results from chapter 2, we can obtain condensed stiffness elemental matrix as:

$$K^{e,condensed}_{c'} = K^e_{c'} - K^e_{up} K^{e-1}_{pp} K^e_{pu} \tag{3.85}$$

In mixed formulation, the same shape functions as used in electrostatic field and displacement finite element formulation will be used to approximate the displacement field in mixed formulation. For stress field(p), shape function for p-1 L^2[19, 20] conforming elements are used. Here, L^2 space is defined as:

$$u \in L^2(\Omega) \ : \ \int_\Omega |u|^2 d\Omega < \infty \tag{3.86}$$

3.5 Benchmark Numerical Example

In this section, we address the question of performance of both displacement finite element formulation and mixed finite element formulation in plain strain and plain stress cases by discussing the convergence of error estimators with h and p refinement for a benchmark problem with known analytical solutions. In this section, the following error measures were investigated.

- L^2 Norm of error in displacement:

$$||\boldsymbol{u} - \boldsymbol{u}_{hp}||_0 = (\int_\Omega |\boldsymbol{u} - \boldsymbol{u}_{hp}|^2 d\Omega)^{1/2} \tag{3.87}$$

- Error measured in the Energy Norm:

$$||\boldsymbol{u} - \boldsymbol{u}_{hp}||_E = (2\mu||\epsilon(\boldsymbol{u} - \boldsymbol{u}_{hp})||_0^2 + \lambda||div(\boldsymbol{u} - \boldsymbol{u}_{hp})||_0^2)^{\frac{1}{2}} \tag{3.88}$$

  which for mixed finite element method becomes:

$$||\boldsymbol{u} - \boldsymbol{u}_{hp}||_E = (2\mu||\epsilon(\boldsymbol{u} - \boldsymbol{u}_{hp})||_0^2 + \lambda^{-1}||p - p_{hp}||_0^2)^{\frac{1}{2}} \tag{3.89}$$

- Error in the sum of normal stress:

$$||\boldsymbol{u} - \boldsymbol{u}_{hp}||_{SNS} = [\int_{\Omega} |(\sigma_{xx} + \sigma_{yy}) - (\sigma_{hp,xx} + \sigma_{hp,yy})|^2 d\Omega]^{\frac{1}{2}} \quad (3.90)$$

Here, $\boldsymbol{u}_{hp}$, p_{hp} and σ_{hp} represent the numerical solution obtained from the hp finite element methods while $\boldsymbol{u}$, p, and σ represent the exact analytical solutions.

3.5.1 Problem description

The problem is illustrated in the Figure(3.1) which is the case of a rigid circular inclusion in an infinite plate subjected to unidirectional tension σ_∞. Because of the symmetry of the plate, one quarter of the domain is considered here. In order to model the problem accurately, a finite element domain is chosen and exact analytical values are applied on Neumann boundary. Here, Young's modulus E is considered as 1, and Poisson's ratio ν is considered as 0.4999 to observe locking phenomena.

3.5.2 Analytical Solution

The exact solution for the plain strain case can be found in the Reference [24]. The exact displacement components which is given in Cylindrical coordinates are:

$$u_r = \frac{\sigma_\infty}{8Gr}\{(\kappa-1)r^2 + 2\gamma a^2 + [\beta(\kappa+1)a^2 + 2r^2 + \frac{2\delta a^4}{r^2}]\cos 2\theta\} \quad (3.91)$$

$$u_\theta = -\frac{\sigma_\infty}{8Gr}[\beta(\kappa-1)a^2 + 2r^2 - \frac{2\delta a^4}{r^2}]\sin 2\theta \quad (3.92)$$

and the exact stress components are:

$$\sigma_r = \frac{\sigma_\infty}{2}[1 - \frac{\gamma a^2}{r^2} + (1 - \frac{2\beta a^2}{r^2} - \frac{3\delta a^4}{r^4})\cos 2\theta] \quad (3.93)$$

$$\sigma_\theta = \frac{\sigma_\infty}{2}[1 + \frac{\gamma a^2}{r^2} - (1 - \frac{3\delta a^4}{r^4})\cos 2\theta] \quad (3.94)$$

$$\tau_{r\theta} = -\frac{\sigma_\infty}{2}(1 + \frac{\beta a^2}{r^2} + \frac{3\delta a^4}{r^4})\sin 2\theta \quad (3.95)$$

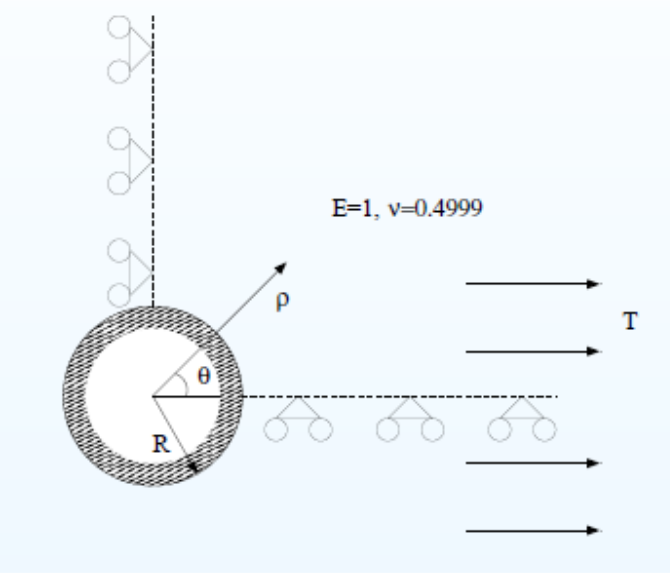

Figure 3.1: Rigid circular inclusion in an infinite plate

where $\kappa,\ \beta,\ \gamma,\ \delta$ are constants which depend on Poisson's ratio ν only. In the case of plain strain:

$$\kappa = 3 - 4\nu, \quad \beta = -\frac{2}{3-4\nu}, \quad \gamma = -\frac{2-4\nu}{2}, \quad \delta = \frac{1}{3-4\nu} \tag{3.96}$$

In plain stress case, the exact solution for displacement and stress components can be expressed as[26]:

$$\begin{aligned}
u_r &= \frac{\sigma_\infty}{2}\left[\frac{r}{2(\hat{\lambda}+\mu)} - \frac{a^2}{2(\hat{\lambda}+\mu)r}\right] \\
&+ \frac{\sigma_\infty}{4\mu r}\left[Ba^2\frac{\hat{\lambda}+2\mu}{\hat{\lambda}+\mu} + r^2 + \frac{Ca^4}{r^2}\right]\cos 2\theta \qquad (3.97)\\
u_\theta &= -\frac{\sigma_\infty}{4\mu r}\left[Ba^2\frac{\mu}{\hat{\lambda}+\mu} + r^2 - \frac{Ca^4}{r^2}\right]\sin 2\theta \qquad (3.98)\\
\sigma_r &= \frac{\sigma_\infty}{2}\left[1 + \frac{\mu a^2}{(\hat{\lambda}+\mu)r^2}\right] + \frac{\sigma_\infty}{2}\left[1 - \frac{2Ba^2}{r^2} - \frac{3Ca^4}{r^4}\right]\cos 2\theta \qquad (3.99)\\
\sigma_\theta &= \frac{\sigma_\infty}{2}\left[1 - \frac{\mu a^2}{(\hat{\lambda}+\mu)r^2}\right] - \frac{\sigma_\infty}{2}\left[1 - \frac{3Ca^4}{r^4}\right]\cos 2\theta \qquad (3.100)\\
\tau_{r\theta} &= -\frac{\sigma_\infty}{2}\left[1 + \frac{Ba^2}{r^2} + \frac{3Ca^4}{r^4}\right]\sin 2\theta \qquad (3.101)
\end{aligned}$$

where B and C are constants which depend on $\hat{\lambda}$ and μ only. B and C is given as:

$$B = \frac{-2(\hat{\lambda} + \mu)}{\hat{\lambda} + 3\mu}, \quad C = \frac{\hat{\lambda} + \mu}{\hat{\lambda} + 3\mu} \tag{3.102}$$

3.5.3 Error Estimate with h, p refinement

We have plotted L_2 norm of error in displacement, error measured in the energy norm, and error in the sum of the normal stresses(SNS), vs. NDF, the number of degrees of freedom. Through these log-log plots, the locking phenomenon and numerical convergence rates are discussed.

Plain Strain Case

Figure(3.2) shows the convergence of $||\boldsymbol{u} - \boldsymbol{u}_{hp}||_0$, $||\boldsymbol{u} - \boldsymbol{u}_{hp}||_E$ and $||\boldsymbol{u} - \boldsymbol{u}_{hp}||_{SNS}$ when uniform h refinement for meshes of quadrilateral and triangular elements is performed with displacement formulation. This figure clearly exhibit the poor convergence behavior of low order elements (p=1). Locking occurs in the sum of normal stresses when p=1 for both quadrilateral and triangular elements. For $p \geq 2$ the expected algebraic rates of convergence are obtained.

Figure(3.3) shows the convergence of $||\boldsymbol{u} - \boldsymbol{u}_{hp}||_0$, $||\boldsymbol{u} - \boldsymbol{u}_{hp}||_E$ and $||\boldsymbol{u} - \boldsymbol{u}_{hp}||_{SNS}$ when uniform h refinement for meshes of quadrilateral and triangular elements is performed with mixed formulation. This figure exhibit the poor convergence behavior of low order elements (p=1) as well. There is still locking in the sum of normal stresses when p=1 for both quadrilateral and triangular elements. However, the magnitude of error in the sum of normal stresses is much smaller than that obtained with displacement formulation. For $p \geq 2$ the expected algebraic rates of convergence are obtained.

The results of p refinement for the displacement formulation are shown in Figure(3.4). From these results, the exponential convergence rates can be observed. Although, the magnitude of the error in the sum of normal stresses is much larger than the other two measures. The error in the sum of normal stresses is nearly 100 when p=1, which is out of tolerant range. Thus there is locking when p=1 for the sum of normal stresses.

The results of p refinement for the mixed formulation are shown in Figure(3.5). These results illustrates the exponential rates of convergence. With mixed formulation, now, the magnitude of the error in the sum of normal stresses when p=1 decreases a lot and is similar to the other two measures.

Figure(3.6) shows the comparison results of the displacement and mixed formulations for p refinement discretised by triangles. From the results, it is observed that there is no locking with either method where the energy norm error is concerned since the curves for $\nu = 0.3$ and $\nu = 0.4999$ are very close. But for the error in the sum of normal stresses, there is marked decrease in accuracy with displacement formulation when Poisson's ratio is from 0.3 to 0.4999. On the other hand, the mixed formulation shows no change as $\nu \rightarrow 0.5$. Hence, no locking can be seen for the mixed formulation for p refinement.

Plain Stress Case

Figure(3.7) shows the convergence of $||\boldsymbol{u} - \boldsymbol{u}_{hp}||_0$, $||\boldsymbol{u} - \boldsymbol{u}_{hp}||_E$ and $||\boldsymbol{u} - \boldsymbol{u}_{hp}||_{SNS}$ when uniform h refinement for meshes of quadrilateral and triangular elements is performed with displacement formulation. The convergence behavior of low order elements is much better than

that in plain strain case. Also, there is no locking in three error measures for both quadrilateral and triangular discretization. For $p \geq 1$ the expected algebraic rates of convergence are obtained.

Figure(3.8) shows the convergence of $||\boldsymbol{u} - \boldsymbol{u}_{hp}||_0$, $||\boldsymbol{u} - \boldsymbol{u}_{hp}||_E$ and $||\boldsymbol{u} - \boldsymbol{u}_{hp}||_{SNS}$ when uniform h refinement for meshes of quadrilateral and triangular elements is performed with mixed formulation. This figure exhibit the much better convergence behavior of displacement and energy norm error for low order elements compared to plain strain case as well. Although there is locking in the sum of normal stresses when p=1 for both quadrilateral and triangular elements. For $p \geq 2$ the expected algebraic rates of convergence are obtained.

The results of p refinement for the displacement formulation are shown in Figure(3.9). From these results, the exponential convergence rates can be observed. Also, the accuracy of the sum of normal stresses is similar to accuracy of the energy norm error.

The results of p refinement for the mixed formulation are shown in Figure(3.10). These results illustrates the exponential rates of convergence. With mixed formulation, the magnitude of the error in the sum of normal stresses is larger than the other two measures when p=1. But from p=2, the error in the sum of normal stresses is similar to the error of the other two measures.

Summary

To conclude the results above, plain strain case suffers from locking more than plain stress case, which is understandable from the theoretical point of view, because in plain strain case, there is no deformation in Z direction, but for plain stress case, it allows the deformation in Z

direction. Mixed hp finite element method(p¿1) is the best choice to be taken since it can overcome locking and at the same time present exponential convergence rate.

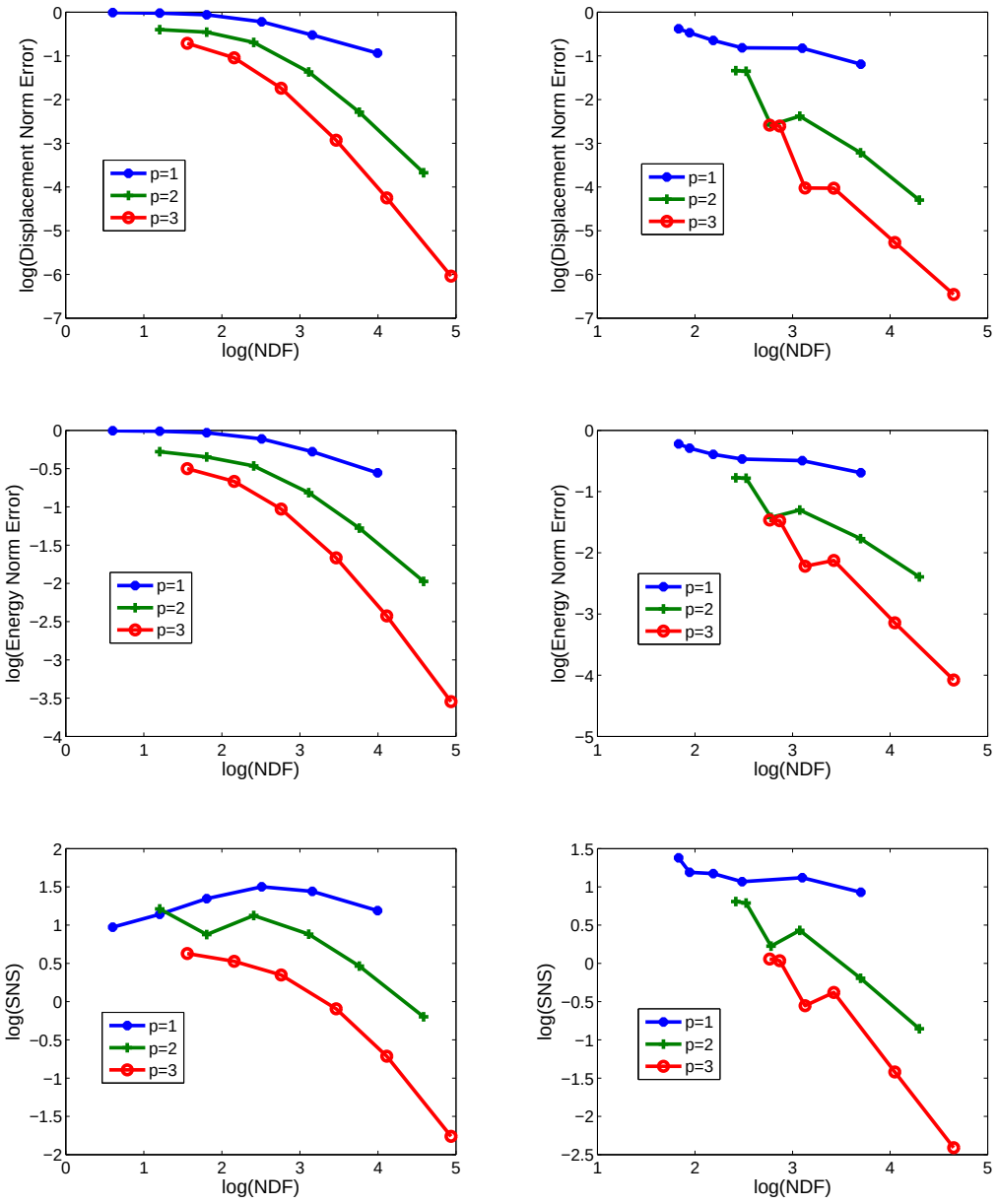

Figure 3.2: Convergence of $||\boldsymbol{u} - \boldsymbol{u}_{hp}||_0$, $||\boldsymbol{u} - \boldsymbol{u}_{hp}||_E$ and $||\boldsymbol{u} - \boldsymbol{u}_{hp}||_{SNS}$ for h refinement using the displacement formulation in plain strain case

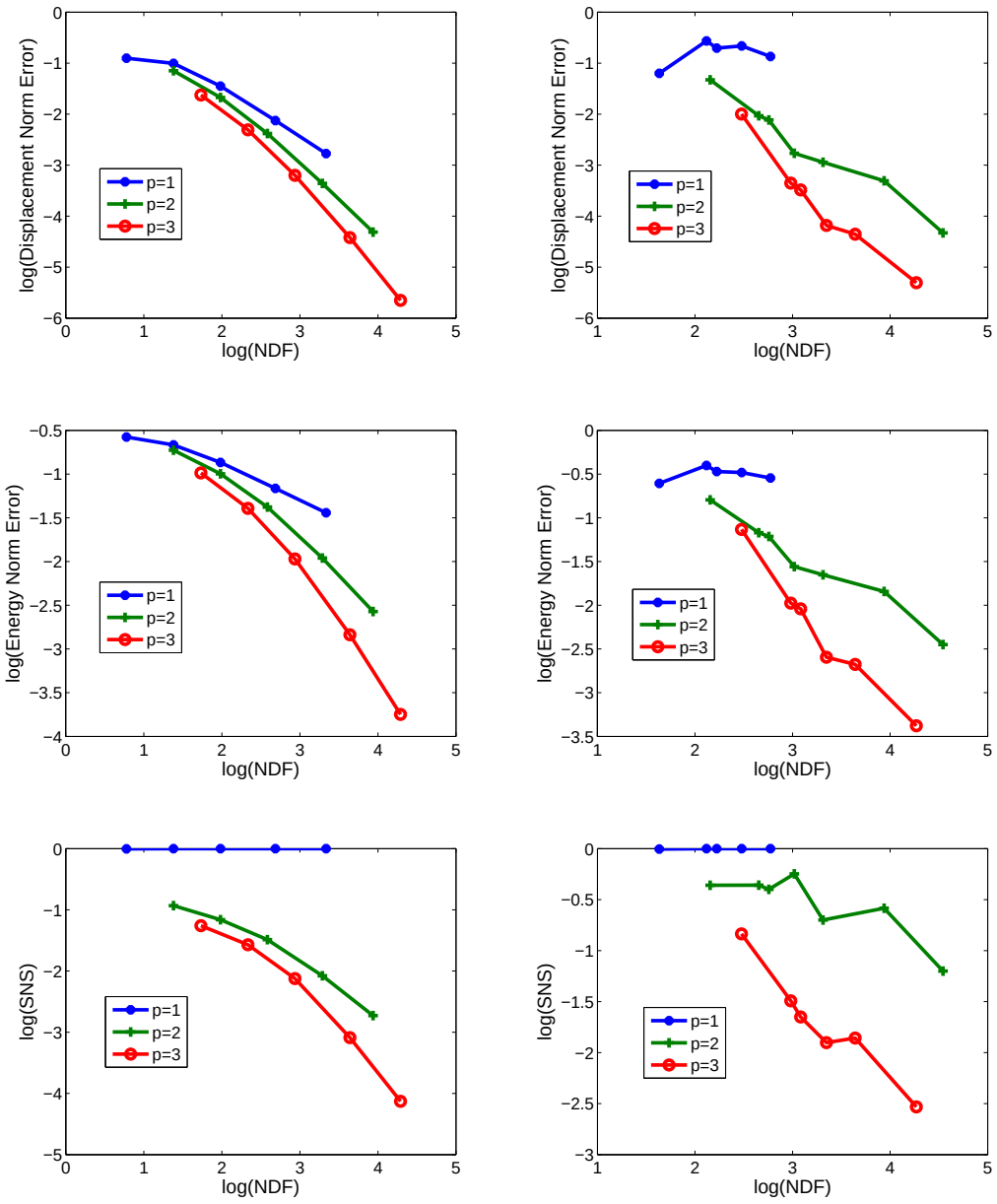

Figure 3.3: Convergence of $||\boldsymbol{u} - \boldsymbol{u}_{hp}||_0$, $||\boldsymbol{u} - \boldsymbol{u}_{hp}||_E$ and $||\boldsymbol{u} - \boldsymbol{u}_{hp}||_{SNS}$ for h refinement using the mixed formulation in plain strain case

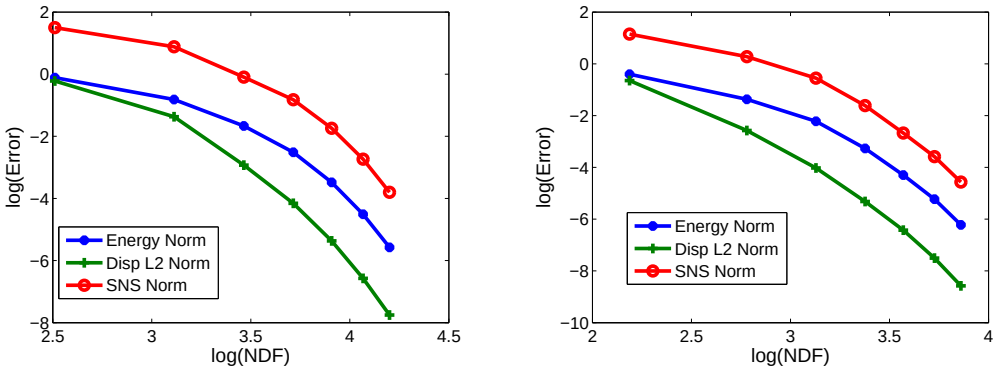

Figure 3.4: Convergence of $||\boldsymbol{u} - \boldsymbol{u}_{hp}||_0$, $||\boldsymbol{u} - \boldsymbol{u}_{hp}||_E$ and $||\boldsymbol{u} - \boldsymbol{u}_{hp}||_{SNS}$ for p refinement using the displacement formulation in plain strain case

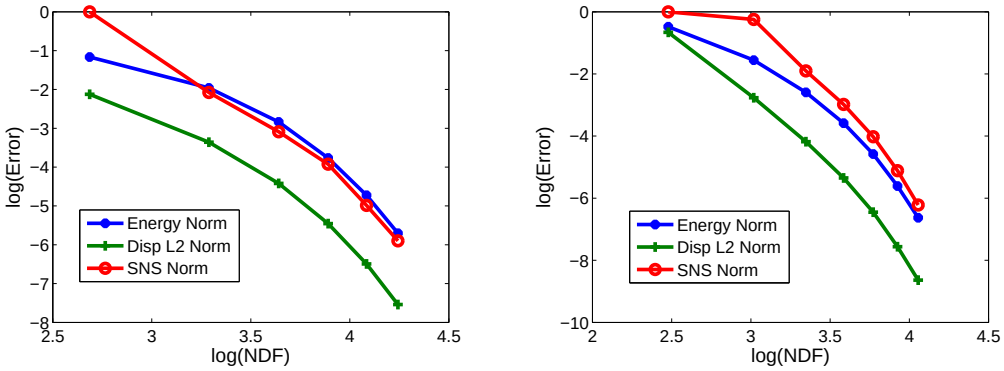

Figure 3.5: Convergence of $||\boldsymbol{u} - \boldsymbol{u}_{hp}||_0$, $||\boldsymbol{u} - \boldsymbol{u}_{hp}||_E$ and $||\boldsymbol{u} - \boldsymbol{u}_{hp}||_{SNS}$ for p refinement using the mixed formulation in plain strain case

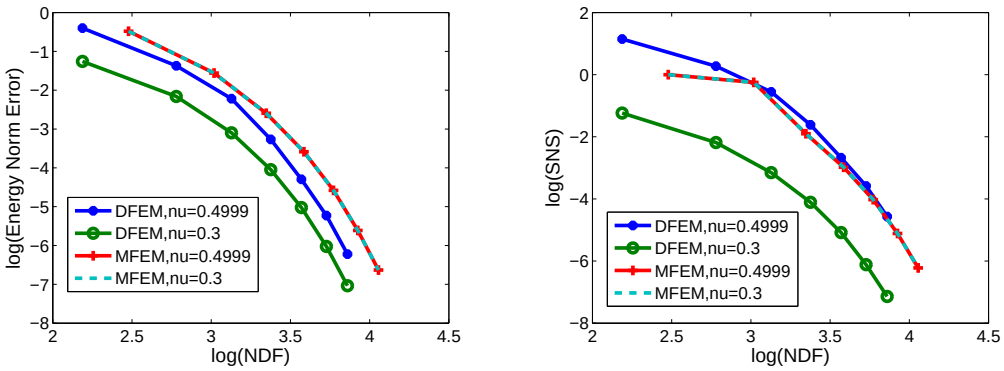

Figure 3.6: Displacement formulation vs. Mixed Formulation for p refinement using triangular elements in plain strain case

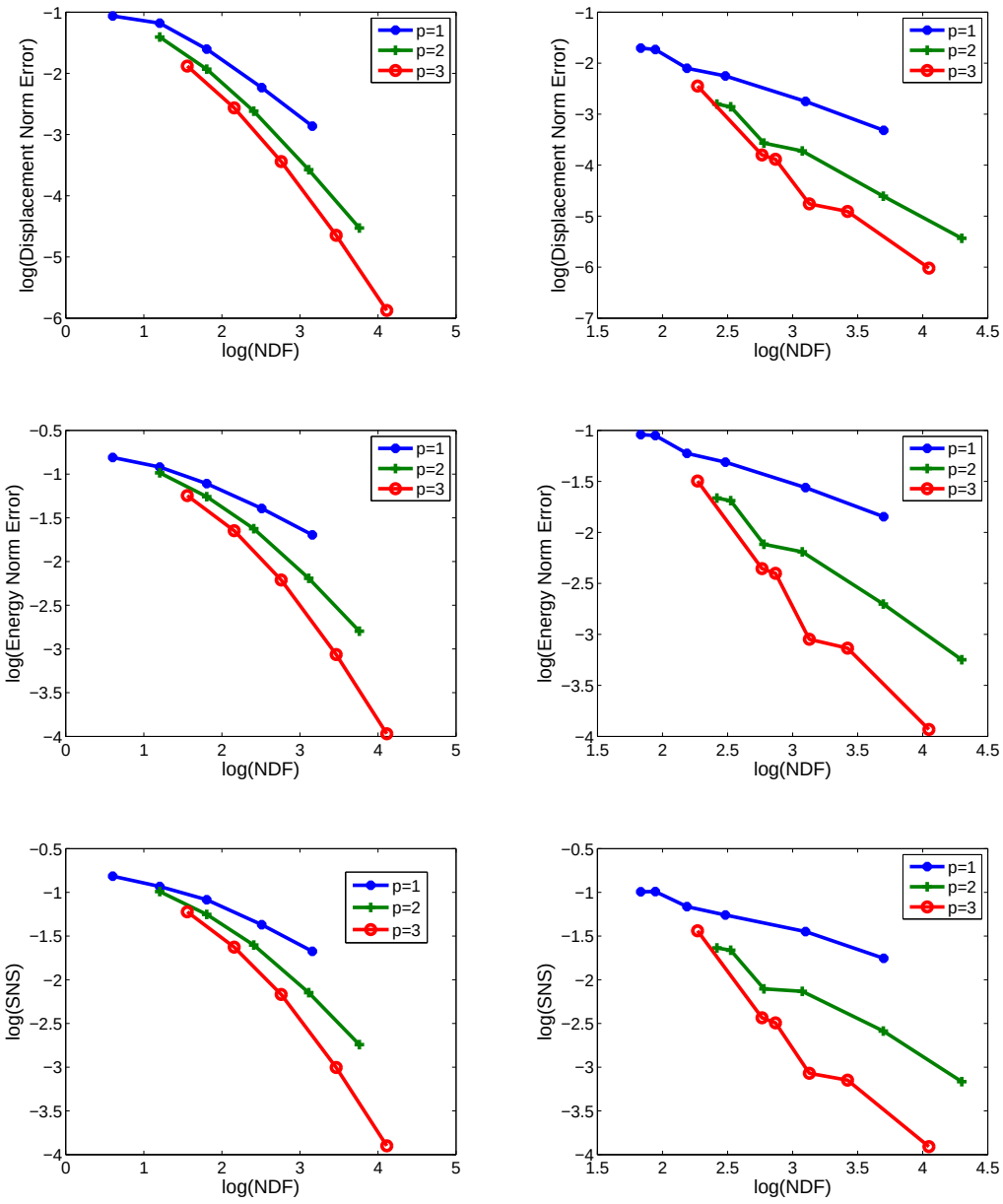

Figure 3.7: Convergence of $||\boldsymbol{u} - \boldsymbol{u}_{hp}||_0$, $||\boldsymbol{u} - \boldsymbol{u}_{hp}||_E$ and $||\boldsymbol{u} - \boldsymbol{u}_{hp}||_{SNS}$ for h refinement using the displacement formulation in plain stress case

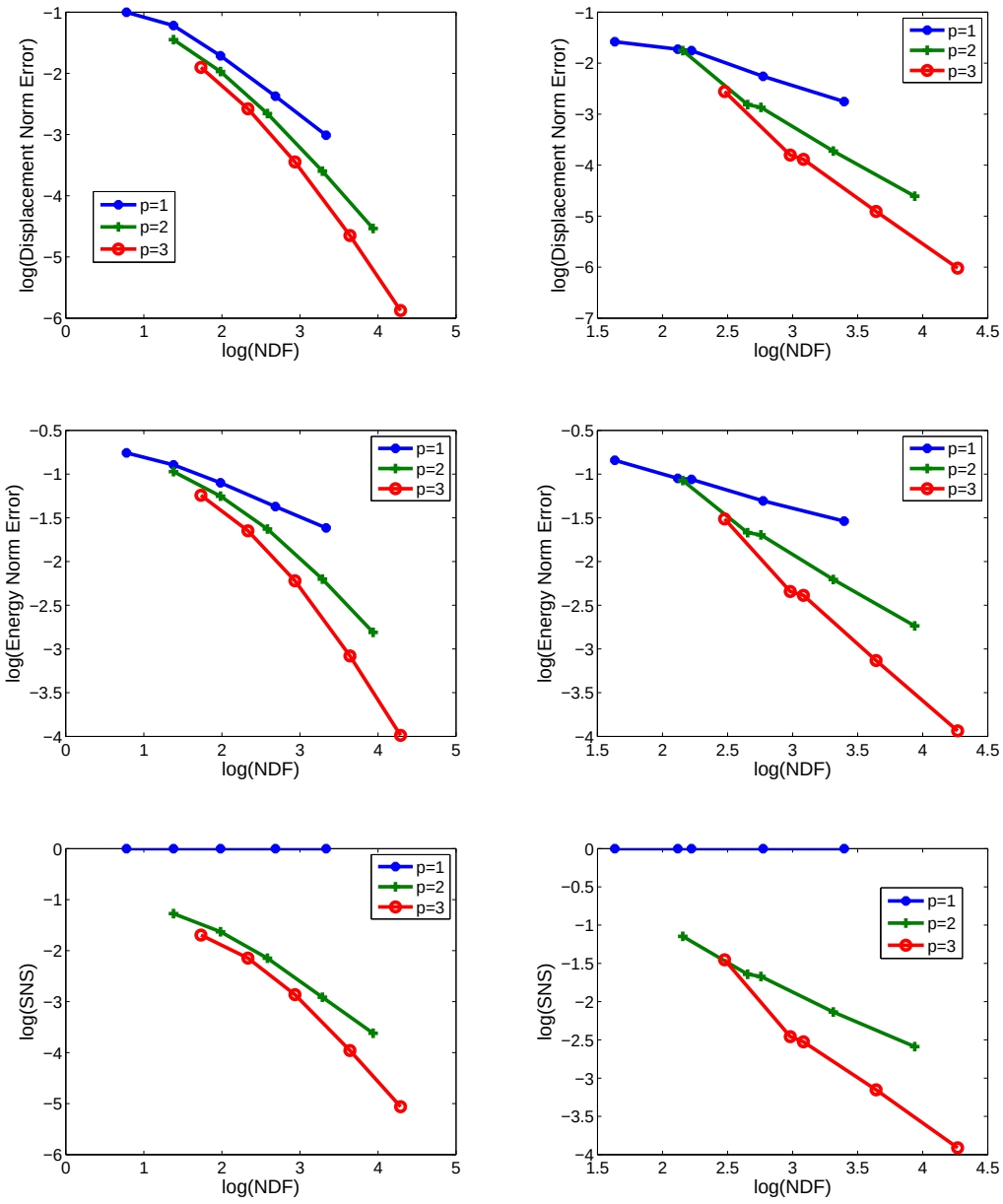

Figure 3.8: Convergence of $||\boldsymbol{u} - \boldsymbol{u}_{hp}||_0$, $||\boldsymbol{u} - \boldsymbol{u}_{hp}||_E$ and $||\boldsymbol{u} - \boldsymbol{u}_{hp}||_{SNS}$ for h refinement using the mixed formulation in plain stress case

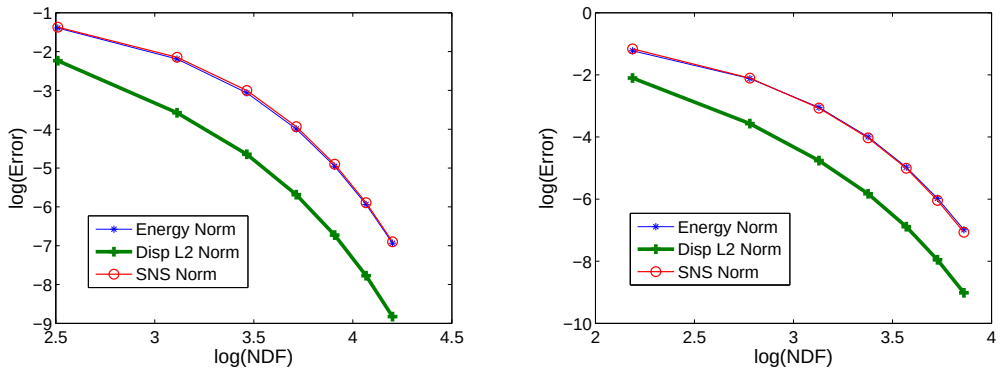

Figure 3.9: Convergence of $||\boldsymbol{u} - \boldsymbol{u}_{hp}||_0$, $||\boldsymbol{u} - \boldsymbol{u}_{hp}||_E$ and $||\boldsymbol{u} - \boldsymbol{u}_{hp}||_{SNS}$ for p refinement using the displacement formulation in plain stress case

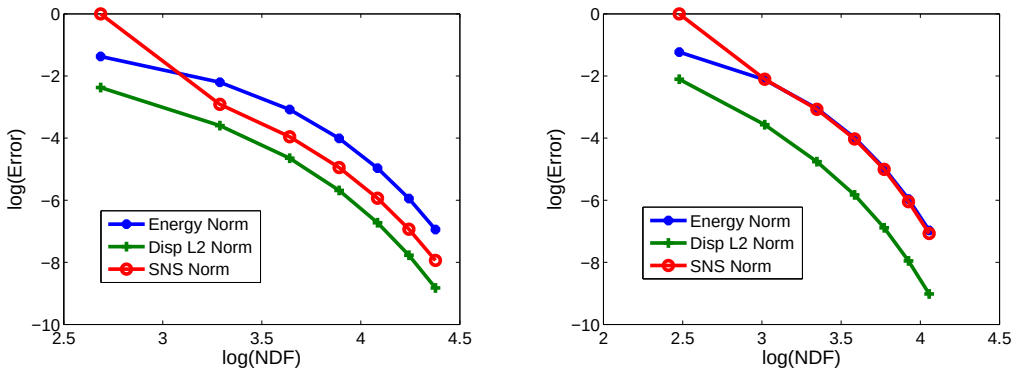

Figure 3.10: Convergence of $||\boldsymbol{u} - \boldsymbol{u}_{hp}||_0$, $||\boldsymbol{u} - \boldsymbol{u}_{hp}||_E$ and $||\boldsymbol{u} - \boldsymbol{u}_{hp}||_{SNS}$ for p refinement using the mixed formulation in plain stress case

Chapter 4

Coupled Electrostatic-Mechanical Problem

As mentioned in chapter 1, this thesis concentrates on electrostriction, one example of coupled electrostatic mechanical behaviors. The key point of electrostriction can be described as: Electric field leads to stresses in the material, which leads to deformation and strains in the material, in turn this leads to changes in the electrical properties of the material. In the previous chapters, we have already discussed electrostatic field and mechanical field separately. In this chapter coupling mechanism between these two fields is discussed. The mathematical principle, coupling algorithms, and simulation results of an electrostriction benchmark are presented in the following sections.

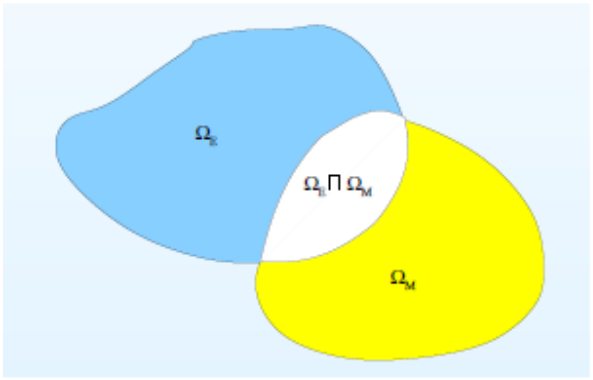

Figure 4.1: Electrostriction problem domain

4.1 Mathematical Theory

The electrostriction problem is considered on the domain shown in Figure(4.1), where Ω_E represents the electric domain, Ω_M is the mechanical domain, and $\Omega_E \cap \Omega_M$ represents the domain where electric field domain and mechanical field domain overlap. The two fields domain can overlap either totally or partially. The coupling occurs only on the overlapping domain.

The electrostatic boundary value problem has been discussed in chapter 2, where we concentrate on the domain consists of a linear, isotropic(but not necessarily homogeneous) medium. So ε is taken as a scalar function of position, which is precise constant. However, for the problem of electrostriction, the overlapping domain doesn't keep isotropic always, which means in the overlapping domain permittivity ε is no longer a precise constant scalar but a tensor that is a function of position. For anisotropic medium, permittivity ε is a second order tensor.This means in two dimensional electrostriction problem with Cartesian coordinates

ε can be expressed as:

$$\varepsilon = \begin{pmatrix} \varepsilon_{11} & \varepsilon_{12} \\ \varepsilon_{21} & \varepsilon_{22} \end{pmatrix} \tag{4.1}$$

In electrostriction, under isothermal conditions the only factors influencing anisotropy are the strains, so that permittivity can be defined as[27]

$$\varepsilon_{ij} = \varepsilon_r^0 \varepsilon_0 \delta_{ij} + \varepsilon_r^1 \varepsilon_0 \epsilon_{ij} + \varepsilon_r^2 \varepsilon_0 \epsilon_{kk} \delta ij, \qquad i, j = 1, 2 \tag{4.2}$$

where ε_0 represents the permittivity when there is no deformation, ε_r^0,ε_r^1 and ε_r^2 are scalar constants determined experimentally, δ_{ij} is the Kronecker delta, and ϵ_{ij} is strain tensor coming from the deformation. The electrostatic stresses can be given as[27]:

$$\sigma_{ij}^E = aE_iE_j + bE_kE_k\delta ij, \qquad i, j = 1, 2 \tag{4.3}$$

where E_i is component of the electrical intensity vector, and a and b are scalar constants defined as[26, 27]:

$$a = (2\varepsilon_r^0 - \varepsilon_r^1)\varepsilon_0/2 \tag{4.4}$$

$$b = -(\varepsilon_r^0 + \varepsilon_r^2)\varepsilon_0/2 \tag{4.5}$$

The electric volume force generated by electric stresses can be expressed as:

$$\boldsymbol{f_v} = \nabla \cdot \boldsymbol{\sigma}^E \tag{4.6}$$

The electric volume force acts as a body force to influence the overlapping domain in the mechanical part.

Therefore, electrostriction boundary problems can be expressed with

following governing equations and boundary conditions[26].

$$\begin{aligned}
\nabla \cdot (\boldsymbol{\varepsilon} \nabla \Phi) &= -\rho_v && in\ \Omega_E \\
\boldsymbol{\varepsilon} &= \varepsilon_r^0 \varepsilon_0 \boldsymbol{I} && in\ \Omega_E - \Omega_M \\
\boldsymbol{\varepsilon} &= \varepsilon_r^0 \varepsilon_0 \boldsymbol{I} + \varepsilon_r^1 \varepsilon_0 \boldsymbol{\epsilon} + \varepsilon_r^2 \varepsilon_0 trace(\boldsymbol{\epsilon}) \boldsymbol{I} && in\ \Omega_E \cap \Omega_M \\
\Phi &= f_D && on\ \Gamma_E^D \\
\boldsymbol{n} \cdot (\boldsymbol{\varepsilon} \nabla \Phi) &= f_N && on\ \Gamma_E^N \\
\boldsymbol{E} &= -\nabla \Phi && in\ \Omega_E \\
\boldsymbol{\sigma}^E &= a \boldsymbol{E} \boldsymbol{E}^{\boldsymbol{T}} + b\ trace(\boldsymbol{E} \boldsymbol{E}^{\boldsymbol{T}}) \boldsymbol{I} && in\ \Omega_E \\
\boldsymbol{f}_v &= \nabla \cdot \sigma^E && in\ \Omega_E
\end{aligned} \tag{4.7}$$

$$\begin{aligned}
\nabla \cdot \boldsymbol{\sigma}^M + \boldsymbol{f} &= 0 && in\ \Omega_M \\
\nabla \cdot \boldsymbol{\sigma}^M &= 0 && in\ \Omega_M - \Omega_E \\
\nabla \cdot (\boldsymbol{\sigma}^M + \boldsymbol{\sigma}^E) &= 0 && in\ \Omega_E \cap \Omega_M \\
\boldsymbol{u} &= \boldsymbol{u}_D && on\ \Gamma_M^D \\
\boldsymbol{n} \cdot (\boldsymbol{\sigma}^M + \boldsymbol{\sigma}^E) &= \boldsymbol{t}_N && on\ \Gamma_M^N \\
\boldsymbol{\sigma}^M &= \boldsymbol{c} : \boldsymbol{\epsilon} && in\ \Omega_M \\
\boldsymbol{\sigma} &= \boldsymbol{\sigma}^M + \boldsymbol{\sigma}^E && in\ \Omega_E \cap \Omega_M
\end{aligned}$$

where σ^M stands for the mechanical stress tensor. Other symbols are already stated before.

4.2 Electrostatic Volume Force Calculation

In general, the electrostatic volume force is obtained by applying the principle of virtual work. The general formula can be found in several references[14, 26], and has the following expression:

$$\boldsymbol{f_v} = \boldsymbol{f_v^1} + \boldsymbol{f_v^2} + \boldsymbol{f_v^3} \tag{4.8}$$

where,

$$\boldsymbol{f_v^1} = \rho_v \boldsymbol{E} \tag{4.9}$$

$$\boldsymbol{f}_{\boldsymbol{v}}^2 = -\frac{1}{2}|\boldsymbol{E}|^2\nabla\varepsilon \tag{4.10}$$

$$\boldsymbol{f}_{\boldsymbol{v}}^3 = \frac{1}{2}\nabla(|\boldsymbol{E}|^2\tau\frac{\partial\varepsilon}{\partial\tau} \tag{4.11}$$

Here, τ represents the density of matter. $\boldsymbol{f}_{\boldsymbol{v}}^1$ is generated due to existence of volume charge, $\boldsymbol{f}_{\boldsymbol{v}}^2$ is generated due to changes in the permittivity, and $\boldsymbol{f}_{\boldsymbol{v}}^3$ is generated due to the deformation of the dielectric.
In this thesis, we use another electrostatic force form instead of general one, whose advantage will be shown in computational implementation.

4.3 Computational Implementation

In the electrostriction problem, when the permittivity is given, then the electrostatic field can be solved through the finite element approach developed in chapter 2. In turn, when body force is given, the mechanical field can be solved through either displacement finite element formulation or mixed finite element formulation developed in chapter 3.
The body force term in the coupled overlapping domain is expressed as $\boldsymbol{f}_v = \nabla\cdot\sigma^E$ and can be implemented as a internal force term described in chapter 3 and applied in the Neumann boundary when solving mechanical field part. The contribution of $\boldsymbol{f}_v$ to the residual force vector in the overlapping domain of mechanical part transforms (3.27) and (3.28) into:

$$T_a^e = \int_{(\Omega_E\cap\Omega_M)_e}\sigma^E\nabla N_a d\Omega \tag{4.12}$$

$$F_a^e = \int_{\partial(\Omega_E\cap\Omega_M)_e} N_a[\boldsymbol{n}\cdot(\sigma^E+\sigma^M)]ds \tag{4.13}$$

From here, we can observe the use of this force calculation method can led to a easy, natural and efficient computational implementation, while other force calculation approaches such as we discussed in previous

section do not. Thus, from the computational point of view, the force calculation approach used in this thesis has considerable advantages.

4.4 Algorithm for Electrostriction Problem

To summarize the theory in previous sections, the work principle of electrostriction behavior can be expressed by the following two algorithms, one way coupling and two way coupling.

4.4.1 One Way Coupling

One way coupling considers the situation when permittivity $\boldsymbol{\varepsilon} = \varepsilon_r^0 \varepsilon_0 \boldsymbol{I}$ in the electrostatic domain and the permittivity is independent to the mechanical field. Then the algorithm can be expressed with following steps.

Step 1: Compute solutions to electrostatic boundary value problem:

$$\begin{aligned} \nabla \cdot (\boldsymbol{\varepsilon} \nabla \Phi) &= 0 \qquad in\ \Omega_E \\ \Phi &= f_D \qquad on\ \Gamma_E^D \\ \boldsymbol{n} \cdot (\boldsymbol{\varepsilon} \nabla \Phi) &= f_N \qquad on\ \Gamma_E^N \end{aligned} \tag{4.14}$$

Step 2: Compute electric field, electric stress tensor and electric force vector in the overlapping domain:

$$\boldsymbol{E} = -\nabla \Phi \qquad in\ \Omega_E \cap \Omega_M \tag{4.15}$$

$$\boldsymbol{\sigma}^E = a \boldsymbol{E} \boldsymbol{E}^{\boldsymbol{T}} + b\ trace(\boldsymbol{E} \boldsymbol{E}^{\boldsymbol{T}}) \boldsymbol{I} \qquad in\ \Omega_E \cap \Omega_M \tag{4.16}$$

$$\boldsymbol{f}_v = \nabla \cdot \sigma^E \qquad in\ \Omega_E \cap \Omega_M \tag{4.17}$$

Step 3: Compute solutions to elastostatic boundary value problem:

$$\nabla \cdot \boldsymbol{\sigma}^M + \boldsymbol{f} = \nabla \cdot \boldsymbol{\sigma}^M = 0 \qquad in\ \Omega_M - \Omega_E \tag{4.18}$$

$$
\begin{aligned}
\nabla \cdot \boldsymbol{\sigma}^M + \boldsymbol{f} &= \nabla \cdot (\boldsymbol{\sigma}^M + \boldsymbol{\sigma}^E) = 0 \qquad in\ \Omega_E \cap \Omega_M && (4.19)\\
\boldsymbol{u} &= \boldsymbol{u}_D \qquad on\ \Gamma_M^D && (4.20)\\
\boldsymbol{n} \cdot (\boldsymbol{\sigma}^M + \boldsymbol{\sigma}^E) &= \boldsymbol{t}_N \qquad on\ \Gamma_M^N && (4.21)\\
& && (4.22)
\end{aligned}
$$

4.4.2 Two Way Coupling

Two way coupling considers real electrostriction problem, where an iterative loop is needed to simulate the coupled behavior.

set i=1 and $\boldsymbol{\varepsilon} = \varepsilon_r^0 \varepsilon_0 \boldsymbol{I}$ in Ω_E

while $||\boldsymbol{\varepsilon}^i - \boldsymbol{\varepsilon}^{i-1}|| > TOL$ do

Step 1: Compute solutions to electrostatic boundary value problem:

$$
\begin{aligned}
\nabla \cdot (\boldsymbol{\varepsilon}^i \nabla \Phi) &= 0 \qquad in\ \Omega_E \\
\Phi &= f_D \qquad on\ \Gamma_E^D && (4.23)\\
\boldsymbol{n} \cdot (\boldsymbol{\varepsilon^i} \nabla \Phi) &= f_N \qquad on\ \Gamma_E^N
\end{aligned}
$$

Step 2: Compute electric field, electric stress tensor and electric force vector in the overlapping domain:

$$
\begin{aligned}
\boldsymbol{E} &= -\nabla \Phi \qquad in\ \Omega_E \cap \Omega_M && (4.24)\\
\boldsymbol{\sigma}^E &= a\boldsymbol{E}\boldsymbol{E}^{\boldsymbol{T}} + b\ trace(\boldsymbol{E}\boldsymbol{E}^{\boldsymbol{T}})\boldsymbol{I} \qquad in\ \Omega_E \cap \Omega_M && (4.25)\\
\boldsymbol{f}_v &= \nabla \cdot \sigma^E \qquad in\ \Omega_E \cap \Omega_M && (4.26)
\end{aligned}
$$

Step 3: Compute solutions to elastostatic boundary value problem:

$$
\begin{aligned}
\nabla \cdot \boldsymbol{\sigma}^M + \boldsymbol{f} &= \nabla \cdot \boldsymbol{\sigma}^M = 0 \qquad in\ \Omega_M - \Omega_E && (4.27)\\
\nabla \cdot \boldsymbol{\sigma}^M + \boldsymbol{f} &= \nabla \cdot (\boldsymbol{\sigma}^M + \boldsymbol{\sigma}^E) = 0 \qquad in\ \Omega_E \cap \Omega_M && (4.28)\\
\boldsymbol{u} &= \boldsymbol{u}_D \qquad on\ \Gamma_M^D && (4.29)\\
\boldsymbol{n} \cdot (\boldsymbol{\sigma}^M + \boldsymbol{\sigma}^E) &= \boldsymbol{t}_N \qquad on\ \Gamma_M^N && (4.30)\\
& && (4.31)
\end{aligned}
$$

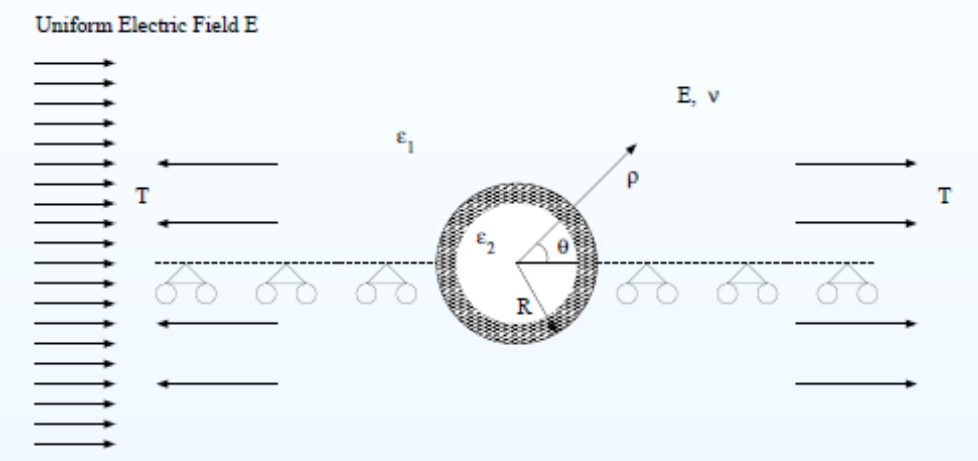

Figure 4.2: Electrostriction benchmark problem

set i=i+1

set:

$$\boldsymbol{\varepsilon} = \varepsilon_r^0 \varepsilon_0 \boldsymbol{I} \qquad in\ \Omega_E - \Omega_M \tag{4.32}$$

$$\boldsymbol{\varepsilon} = \varepsilon_r^0 \varepsilon_0 \boldsymbol{I} + \varepsilon_r^1 \varepsilon_0 \boldsymbol{\epsilon} + \varepsilon_r^2 \varepsilon_0 trace(\boldsymbol{\epsilon}) \boldsymbol{I} \qquad in\ \Omega_E \cap \Omega_M \tag{4.33}$$

end while

4.5 Electrostriction Benchmark Example

4.5.1 Benchmark Problem Description

The problem is illustrated in Figure(4.2), which is the case of infinite plate with rigid dielectric insert subjected to unidirectional tension (T) and uniform electric field (E_∞) in the infinity. In order to simulate the coupled behavior accurately, a finite domain from the infinite

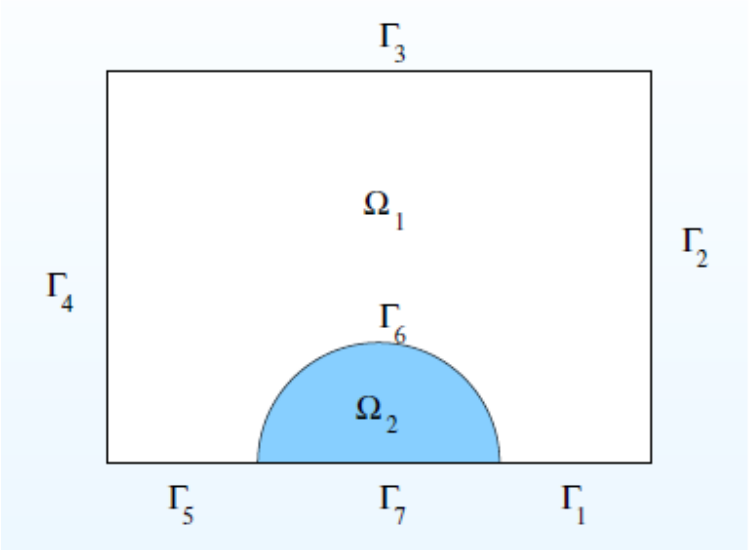

Figure 4.3: Electrostriction finite domain

plate is selected and exact analytical value is applied on both Neumann and Dirichlet boundaries. The finite domain selected is shown in Figure(4.3) and electrical and mechanical domains are defined according to the real problem, respectively.

The electric domain consists of following domains and boundaries.

$$\begin{aligned} \Omega_E &= \Omega_1 \cup \Omega_2 \\ \partial\Omega_E &= \Gamma_1 \cup \Gamma_2 \cup \Gamma_3 \cup \Gamma_4 \cup \Gamma_5 \cup \Gamma_7 \end{aligned}$$

The mechanical domain consists of following domains and boundaries.

$$\begin{aligned} \Omega_M &= \Omega_1 \\ \partial\Omega_M &= \Gamma_1 \cup \Gamma_2 \cup \Gamma_3 \cup \Gamma_4 \cup \Gamma_5 \cup \Gamma_6 \end{aligned}$$

For one way coupling case, the following values are chosen to simulate

the problem.

$$E_\infty = E_x^\infty = 1 \tag{4.34}$$

$$\varepsilon_r^0 = \begin{matrix} 2 & in & \Omega_1 \\ 1 & in & \Omega_2 \end{matrix} \tag{4.35}$$

$$E_y = 1 \quad , \quad \nu = 0.4999 \tag{4.36}$$

where, E_∞ is the electric field in infinity, ε_r^0 is a scalar constant determined experimentally, E_y is Young's modulus and ν is Poisson's ratio. For the two way coupling algorithm, material called MP1880 film is employed to model the real problem. The values of parameters of the material are from the reference[28].

$$E_\infty = E_x^\infty = 10^7 Vm^{-1} \tag{4.37}$$

$$\begin{matrix} \varepsilon_r^0 = 2 & \varepsilon_r^1 = -4 & \varepsilon_r^2 = -12 & \Omega_1 \\ \varepsilon_r^0 = 1 & \varepsilon_r^1 = 0 & \varepsilon_r^2 = 0 & \Omega_2 \end{matrix} \tag{4.38}$$

$$E_y = 7.1 \times 10^5 pa, \qquad \nu = 0.4999 \tag{4.39}$$

4.5.2 Analytical Solution

The analytical solution[26] is available for one way coupling case. The main derivation steps are stated below.

Define:

$$E_x + iE_y = -\bar{w'}(Z) \tag{4.40}$$

where $w(Z) = w(x + iy)$ is the solution of the electrostatic problem, and can be expressed as:

$$w(\zeta) = -R\bar{\boldsymbol{E}}_{\boldsymbol{\infty}}\zeta + RA\boldsymbol{E}_{\boldsymbol{\infty}}\zeta^{-1} \qquad for\ |\zeta| > R \tag{4.41}$$

$$w(\zeta) = -BR\zeta\bar{\boldsymbol{E}}_{\boldsymbol{\infty}} \qquad for\ |\zeta| < R \tag{4.42}$$

where,

$$A = \frac{\varepsilon_2 - \varepsilon_1}{\varepsilon_1 + \varepsilon_2} \tag{4.43}$$

$$B = \frac{2\varepsilon_1}{\varepsilon_1 + \varepsilon_2} \tag{4.44}$$

The stresses are obtained for:

$$\sigma_{xx} + \sigma_{yy} = 4Kw^{'}(Z)\bar{w^{'}}(Z) + 4(\varphi^{'}(Z) + \bar{\varphi^{'}}(Z)) \tag{4.45}$$

$$\sigma_{yy} - \sigma_{xx} + 2i\sigma_{xy} = 4Kw^{''}(Z)\bar{w}(Z) + 4(\bar{Z}\varphi^{''}(Z) + \psi^{'}(Z)) \tag{4.46}$$

where

$$\varphi(\zeta) = \Gamma R\zeta + \varphi_0(\zeta) \tag{4.47}$$

$$\psi(\zeta) = R\Gamma^{'}\zeta + \psi_0(\zeta) \tag{4.48}$$

and

$$\kappa = 3 - 4\nu \qquad for\ plain\ strain \tag{4.49}$$

$$\kappa = \frac{3-\nu}{1+\nu} \qquad for\ plain\ stress \tag{4.50}$$

and

$$K = \frac{1}{8}\frac{1-2\nu}{1-\nu}(a+2b) \qquad plain\ strain \tag{4.51}$$

$$K = \frac{1}{8}\frac{\lambda+2\mu}{2\lambda+2\mu}(a+2b) \qquad plain\ stress \tag{4.52}$$

Finally, $\varphi_0(\zeta)$ and $\psi_0(\zeta)$ can be determined as:

$$\varphi_0(\zeta) = \frac{1}{\kappa}(\frac{\bar{\Gamma}^{'}R}{\zeta} - \frac{KE_\infty^2 AR}{\zeta} + \frac{1}{4}\frac{aRE_\infty^2}{\zeta}) \tag{4.53}$$

$$\begin{aligned}\psi_0(\zeta) &= \frac{\bar{\Gamma}R(\kappa-1)}{\zeta} - \frac{1}{\zeta}\psi_0^{'}(\zeta) - \frac{KRE_\infty^2 A}{\zeta^3} - \frac{KRE_\infty \bar{E_\infty}}{\zeta} \\ &+ \frac{KA^2 RE_\infty \bar{E_\infty}}{\zeta} + \frac{1}{12a}\frac{RA^2E_\infty^2}{\zeta^3} + \frac{E_\infty \bar{E_\infty} ARa}{2\zeta}\end{aligned} \tag{4.54}$$

with constants:

$$\Gamma = \bar{\Gamma} = \frac{T}{8} - \frac{KE_\infty \bar{E_\infty}}{2} \tag{4.55}$$

$$\Gamma^{'} = \bar{\Gamma^{'}} = -\frac{T}{4} \tag{4.56}$$

4.5.3 Numerical Results and Error Estimate

For one way coupling, the exact analytical solution can be provided to verify the performance of overall hp finite element formulation for both plain strain case and plain stress case. For two way coupling, there is no exact analytical solution to compare with numerical one. However, comparing with the analytical solution for one way coupling, the limitation of exact solution is investigated.

One Way Coupling

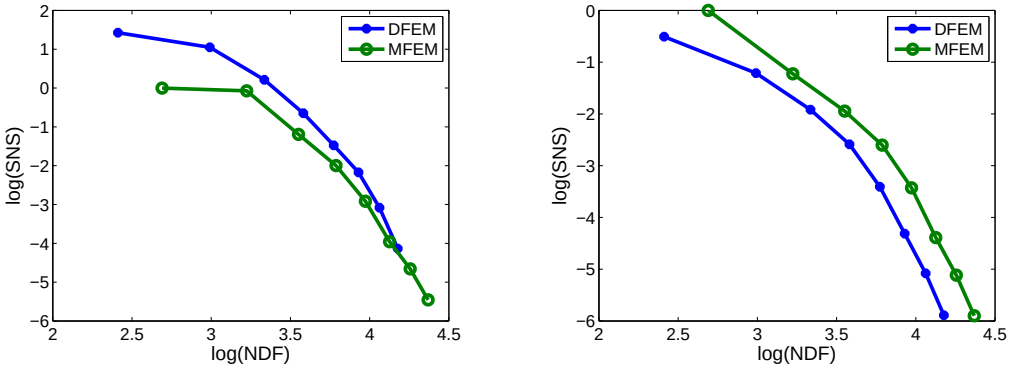

Figure 4.4: Convergence of $||\boldsymbol{u} - \boldsymbol{u}_{hp}||_{SNS}$ for p refinement in plain strain and plain stress cases

Figure(4.4) shows p refinement for the plain strain case and plain stress case with both formulations. In this one way coupling problem, we have smooth solution over the whole domain. Therefore, p refinement is more effective to achieve the accuracy. As expected, both displacement formulation and mixed formulation present exponential convergence rate in plain strain and plain stress cases. But again, we observe there is locking for displacement formulation when p=1.

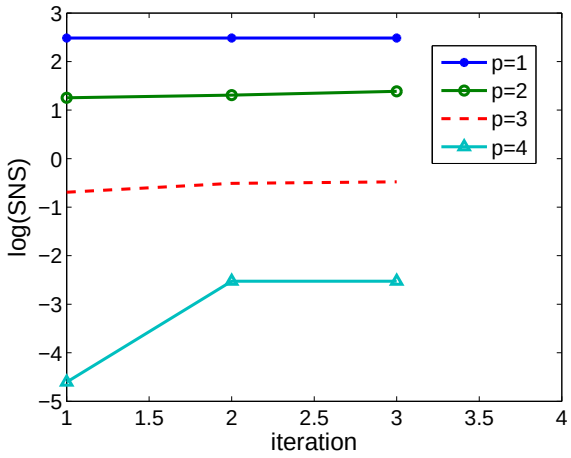

Figure 4.5: $||\boldsymbol{u} - \boldsymbol{u}_{hp}||_{SNS}$ vs. iteration

Two Way Coupling

In the two way coupling, as mentioned before, the analytical solution is not available. Therefore, we cannot obtain convergence performance of our hp approach for two way coupling. However, two way coupling represents the real electrostriction problem. Figure(4.5) shows the changes in the $||\boldsymbol{u} - \boldsymbol{u}_{hp}||_{SNS}$ when compared with analytical solution for one way coupling, with iteration steps. The figure illustrates divergence performance, the error increases with iteration steps and becomes flat. This is because in every iteration step, we use same analytical solution to compare, but in reality, the analytical solution doesn't match the real problem. However, from the divergence figure, we can observe how far away the numerical solution of two way coupling is from the analytical solution of one way coupling.

Chapter 5

Conclusion and Future Work

Coupled electrostatic mechanical behavior has been found in various applications. The real challenge is modeling and analysis of coupling behavior, because the coupling mechanism is highly nonlinear and analytical solutions are not available in most cases. To obtain an accurate prediction of the coupling behavior, appropriate numerical methods are needed. Finite element method(FEM) is a very powerful numerical tool used to simulate and analyze virtually all engineering problems. Therefore, it is employed by engineers to model coupling behavior.

In this thesis, electrostriction, based on the fundamental mechanism of electromechanical coupling, is considered. The key coupling in electrostriction is: stress tensor depends on the permittivity and the permittivity is affected by the strain field. In order to simulate the coupling behavior accurately with finite element method, this research carried out simulation of electric field and mechanical field separately first, making sure simulation of both fields work properly, then combining the two fields together to carry out the simulation of coupling mechanism.

For simulation of electric field, higher order hierarchic shape functions

for order p H^1 conforming elements[19, 20] are employed to implement hp adaptive finite element formulation in MATLAB. When the solution has singularities in some certain points, the choice of h refinement with low order is more effective, but even so, only algebraic convergence rate can be obtained. If the solution is smooth, then p refinement can present exponential convergence rate. Otherwise, only combined hp FEM can achieve exponential convergence rate. For the benchmark problem in electric field, the solution has singularities in the two corners, the developed hp FEM presented algebraic convergence rate as expected with either h or p refinement. If we use nonuniform mesh instead of uniform mesh to generate finer mesh near the two corners, then with p refinement, the developed approach is supposed to present exponential convergence rate. But due to time constraint, only idea is shown.

The mechanical field is simulated on both displacement based finite element formulation and mixed finite element formulation. In displacement formulation, the same shape functions as in electric field are employed. In mixed formulation, not only the same shape functions for order p H^1 conforming elements but also shape functions for order p-1 L^2 conforming elements are employed[19, 20]. There is volumetric locking when Poisson's ratio ν is close to 0.5 in displacement formulation. To overcome locking problem, this thesis adopted mixed formulation. Both formulations are implemented to hp FEM MATLAB code and tested to solve a benchmark problem in plain strain case and plain stress case. For this benchmark problem, with h refinement, both displacement and mixed FEM lock for lower order element (p=1) in plain strain case, and in plain stress, displacement formulation doesn't lock, but mixed formulation presented locking for p=1. Both methods pre-

sented algebraic convergence rate from p=2. With p refinement, in plain strain case, exponential convergence rate can be obtained in both methods. However, the magnitude of the error in the sum of normal stresses is much larger than the other two measures(displacement L2 norm and energy norm) with displacement formulation and locking occurs for p=1. With mixed method, we can overcome locking for p=1, also the magnitude of the sum of normal stresses is similar to that obtained from the other two measures. In plain stress case, no locking occurs with both methods, and both methods presented exponential convergence rate. Moreover, comparing with the results when there is no locking($\nu = 0.3$), we found mixed FEM is more accurate than displacement FEM. To conclude, hp mixed FEM ($p \geq 2$) is the best choice to simulate mechanical field accurately, because we can obtain exponential convergence rate, and no locking occurs as well.

For the simulation of electrostriction, this thesis investigated two coupling algorithms called one way coupling and two way coupling, respectively. One way coupling is the case described as: The stress tensor depends on the permittivity, but permittivity is independent to mechanical field. Two way coupling is for the real electrostriction problem where not only does stress depend on the permittivity, but also permittivity depends on the strain field. The electric field and the mechanical field of electrostriction are implemented using the same hp approach as investigated earlier and coupling mechanism is implemented to obtain integrated hp FEM for the electrostriction. Then it is tested to solve a benchmark problem. With one way coupling algorithm, analytical solution is available, and hp FEM presented exponential convergence rate for p refinement in both plain strain and plain stress cases. For two way coupling algorithm, there is no analytical solution available so

far, however, it represents real electrostriction problem. So this thesis still presented divergence of the approach with p refinement by comparing it with the analytical solution of one way coupling. The results show that the sum of norm of stresses increases with iteration steps and become flat after one or two iterations. However, from the divergence figure, we can observe how far away the numerical solution of two way coupling is from the analytical solution of one way coupling.

In conclusion, hp adaptive finite element method for two dimensional electrostriction is developed successfully in this thesis and accuracy of the approach is demonstrated through some benchmark problems with known analytical solutions. Because of the lack of analytical solution, this thesis doesn't present the convergence of the approach in two way coupling, but still results from the other benchmark problems show the approach developed in this thesis is robust and can be extended to many other applications.

On going work include application to realistic complicated geometries, extension to three dimensional electrostriction and extension to other kinds of coupling problems such as magneto-mechanical coupling.

Bibliography

[1] O.C. Zienkiewicz and R.L. Taylor, *The Finite Element Method*, Vol. 1, 4th Edition, McGRAW-Hill, London, 1989.

[2] Paul Lethbridge, *Multiphysics Analysis*, American Institute of physics, http://www.aip.org/tip/inphfa/vol-10/iss-6/p26.html.

[3] M. Wackerle1, M. Richter1, A. Drost1, and U. Schaber1, *A bi-directional micro pump for the handling of liquids and gases*, Actuator 2004, 9th International Conference on New Actuators, Bremen, Germany, June 14-16 2004, pp. 216.

[4] R Zengerle, S. Kluge, M. Richter, and A.Richter, *A Bidirectional Silicon Micropump*, in Proc. IEEE Micro-Electro-Mechanical Syst, 1995, 0-7803-2503-6.

[5] Dana Dudley, Walter Duncan, and John Slaughter, *Emerging Digital Micromirror Device(DMD) Applications*, Proc. SPIE, Vol. 4985, 14 (2003); doi:10.1117/12.480761.

[6] Wenjing Ye, Subrata Mukherjee, and Noel C. MacDonald, *Optimal Shape Design of an Electrostatic Comb Drive in Microelectromechanical Systems*, Journal OF MicorElectroMechanical System, VOL. 7, NO. 1, MARCH 1998.

[7] R.A. Coutu Jr. and P.E. Kladitis, *A Comparison of Micro-switch Analytic, Finite Element, and Experimental Results*, Sensors and Actuators A 115 (2004) pp 252C258.

[8] Rattikorn Yimnirun, Sylvie M.-L. Eury, V. Sundar, Paul J. Moses, Sei-Joo Jang and Robert E. Newnham, *Electrostriction Measurements on Low Permittivity Dielectric Materials*, Journal of the European Ceramic Society 19 (1999), pp 1269-1273.

[9] S.K.Chakarborty, Dharsa, and Howrah, *Some Two-Dimensional Problems of Electrostriction with Circular Hole*, 1972.

[10] D. K. Vu, P. Steinmann. and G. Possart, *Numerical modelling of non-linear electroelasticity*, International Journal for Numerical Methods in Engineering, 2007, pp 685C704.

[11] JingboZhaoa and Shaobo Qua, *Preparation and temperature dependence of electrostriction properties for PMN-based composite ceramics*, Materials Science and Engineering B 162, (2009), pp 9C13.

[12] Zhicheng Lai, *Finite element analysis of electrostatic coupled systems using geometrically nonlinear mixed assumed stress finite elements*, Master thesis, University of Pretoria, June 2007.

[13] Joaquim Peir and Spencer Sherwin, *Finite Difference, Finite Element and Finite Volume Methods for Partial Differential Equations*, handbook, Department of Aeronautics, Imperial College, London, UK

[14] M.Kaltenbacher, *Numerical Simulation of Mechatronic Sensors and Actuators*, 2nd Edition, Springer, 2007.

[15] Luis E. Garcia-Castillo, *A two-dimensional self-adaptive hp finite element method for the characterization of waveguide discontinu-*

ities. Part I: Energy-norm based automatic hp-adaptivity, Comput. Methods Appl. Mech. Engrg. 196, (2007), pp 4823C4852.

[16] J.C. Maxwell, *A Treatise on Electricity and Magnetism*, vol. I, Dover, 1954.

[17] J.C. Maxwell, *A Treatise on Electricity and Magnetism*, vol. II, Dover, 1954.

[18] P.D. Ledger, *Computational Electromagnetics Lecture Notes*, Swansea University, Swansea UK, 2009.

[19] J. Schoberl and S. Zaglmayr, *High order Nedelec elements with local complete sequence properties*, International Journal for Computation and Mathematics in Electrical and Electronic Engineering(COMPEL), 24:374-384, 2005.

[20] S. Zaglmayr, *High Order Finite Element Methods for Electromagnetic Field Computation*, PhD thesis, Institut fur Numerische Mathematik, Johannes Kepler Univeritat Linz, Austria, 2006.

[21] *Lecture Notes on Numerical Methods for Partial Differencial Equations*, UPC, Spain, 2008.

[22] P.D. Ledger, *Hp-adaptive finite element procedure for electromagnetic scattering problems* , PhD thesis, Swansea University, Swansea UK, 2001.

[23] Javier Bonet and Richard D. Wood, *Nonlinear continuum mechanics for finite element analysis*, 1st edition, Cambridge, 1997.

[24] Lawrence Chilton and Manil Suri, *on the Selection of A Locking-Free hp Element for Elasticity Problems*, International Journal for Numerical Methods in Engineering, Vol. 40, 1997, 2045-2062.

[25] A.J. Gil, *Notes on Locking and Mixed Formulation*, Swansea University, Swansea UK, 2010.

[26] A.J. Gil and P.D. Ledger, Paper in the proceeding, 2010.

[27] R.J. Knops, *Two-Dimensional Electrostriction*, Quart. Journ. Mech. and Applied Math., Vol. XVI, pT. 3, 1963.

[28] Yuri M. Shkel and Daniel J. Klingenberga, *Material parameters for electrostriction*, J. Appl. Phys. 80 (8), 15 October 1996.